Tungsten (VI) speciation in hydrothermal solutions up to 400°c as revealed by in-situ Raman spectroscopy

Carocci, E.; Truche, L.; Cathelineau, M.; Bazarkina, E.;

Originally published:

January 2022

Geochimica et Cosmochimica Acta 317(2021)15, 306-324

DOI: https://doi.org/10.1016/j.gca.2021.11.004

Perma-Link to Publication Repository of HZDR:

https://www.hzdr.de/publications/Publ-33405

Journal Pre-proofs

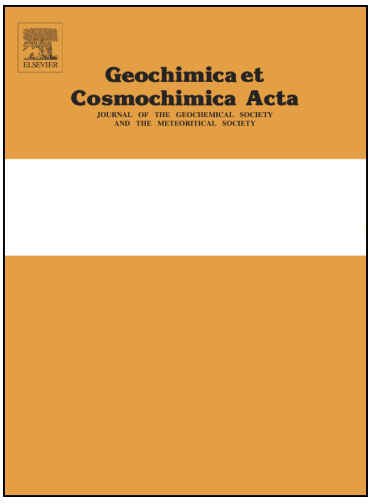

TUNGSTEN (VI) SPECIATION IN HYDROTHERMAL SOLUTIONS UP TO 400°C AS REVEALED BY IN-SITU RAMAN SPECTROSCOPY

Eleonora Carocci, Laurent Truche, Michel Cathelineau, Marie-Camille Caumon, Elena F. Bazarkina

PII: S0016-7037(21)00649-9
DOI: https://doi.org/10.1016/j.gca.2021.11.004
Reference: GCA 12438

To appear in: *Geochimica et Cosmochimica Acta*

Received Date: 21 April 2021
Revised Date: 22 October 2021
Accepted Date: 2 November 2021

Please cite this article as: Carocci, E., Truche, L., Cathelineau, M., Caumon, M-C., Bazarkina, E.F., TUNGSTEN (VI) SPECIATION IN HYDROTHERMAL SOLUTIONS UP TO 400°C AS REVEALED BY IN-SITU RAMAN SPECTROSCOPY, *Geochimica et Cosmochimica Acta* (2021), doi: https://doi.org/10.1016/j.gca.2021.11.004

TUNGSTEN (VI) SPECIATION IN HYDROTHERMAL SOLUTIONS UP TO 400°C AS REVEALED BY IN-SITU RAMAN SPECTROSCOPY

Eleonora Carocci [a, b]*, Laurent Truche [c], Michel Cathelineau [a], Marie-Camille Caumon[a], and Elena F. Bazarkina [d, e, f, g]

[a] *Univ. Lorraine, GeoRessources, CNRS, 54000, Nancy, France*

[b] *Department of Earth and Environmental Sciences, Ludwig-Maximilians-Universität, Theresienstraße 41, München 80333, Germany*

[c] *Univ. Grenoble Alpes, CNRS, ISTERRE, F-38041 Grenoble, France*

[d] *Univ. Grenoble Alpes, CNRS, INSTITUT NÉEL, 25 Avenue des Martyrs, F-38042 Grenoble Cedex 9, France*

[e] *Institute of Geology of Ore Deposits, Petrography, Mineralogy and Geochemistry, Russian Academy of Sciences (IGEM RAS), 35 Staromonetny per., Moscow 119017, Russia*

[f] *The Rossendorf Beamline at ESRF, The European Synchrotron, CS40220, 38043 Grenoble Cedex 9, France*

[g] *Institute of Resource Ecology, Helmholtz Zentrum Dresden-Rossendorf (HZDR), PO Box 510119, 01314 Dresden, Germany*

* Email: eleonora.carocci@min.uni-muenchen.de

Keywords:

Tungsten polymers; Polytungstates, Fused silica glass capillary technique; Ore deposits

Abstract

Tungsten (VI) speciation in hydrothermal solutions is investigated through in-situ Raman spectroscopy coupled with the fused silica glass capillary technique at temperatures up to 400 °C. The effect of temperature, pH, chlorinity and carbonate speciation are evaluated. At all investigated temperatures, the tungstate ion WO_4^{2-} (927 cm^{-1}) is the only W species in solution at pH > 10. At a given pH, the presence of dissolved carbonates and chloride does not affect the tungsten speciation. Tungsten polymers remain stable up to 400 °C under acidic to circum-neutral pH conditions and total tungsten concentration above 0.01 $mol{\cdot}kg_{H2O}^{-1}$. Among the three observed polymers, namely $[W_7O_{24}]^{6-}$ (paratungstate-A, ~ 960 cm^{-1}), $[W_{10}O_{32}]^{4-}$ (tungstate-Y, ~ 970 cm^{-1}), and α-$[H_2W_{12}O_{40}]^{6-}$ (α-metatungstate, ~ 990 cm^{-1}), only the hepta- and dodeca-tungstate are stable at elevated temperature. Combined with revised literature data, these results allow the thermodynamic stability constants of these W polymers to be constrained, enabling quantitative predictions of their relative abundance at temperatures up to 300 °C. These predictions suggest that W polymerization occurs under hydrothermal conditions even at low W concentration (down to 10^{-5} $mol{\cdot}kg_{H2O}^{-1}$) under acidic conditions. These observations imply that the currently available geochemical models on W transport and deposition in deep and hot geological fluids need to be revised.

1. Introduction

The knowledge of tungsten (W) speciation in hydrothermal solutions is of primary importance to develop geochemical models for tungsten ore deposits genesis. W mobility in deep and hot geological fluids is currently poorly constrained despite a consensus that W is predominantly transported in the ore-forming fluids as W(VI) anions with negligible chloride complexation. The few rare models of hydrothermal transport and deposition of tungsten are based on tungsten speciation dominated by tungstic acid ($H_2WO_4^0$) and its dissociation products HWO_4^- and WO_4^{2-} (Heinrich, 1990; Gibert et al., 1992, Wood and Samson, 2000). This relatively simple aqueous W speciation model at elevated temperature (T) and pressure (P) mainly relies on the interpretation of data on W-bearing minerals solubility from quench experiments available at that time (Eugster and Wilson, 1985; Wood and Vlassopoulos, 1989; Wood, 1992). Wang et al. (2019) recently investigated W solubility and speciation in NaCl-bearing solutions up to 350 °C through quenched solution analysis. They demonstrated that NaCl concentration does not affect the solubility of tungsten trioxide. They also concurred with a W speciation dominated by monomeric tungstate species over the entire pH range at T up to 350 °C.

This view of W speciation under hydrothermal condition contrasts with the already well-studied W speciation at ambient T-P, where the coexistence of several polyanions containing 6, 7, 10, and even 12 W-atoms depending on pH is demonstrated (Duncan and Kepert, 1961; Aveston, 1964; Arnek and Sasaki, 1974; Häufe, 1982; Ng and Gulari, 1984; Cruywagen and Van Der Merwe, 1987; Gumerova and Rompel, 2020). It also ignores or simplifies the conclusions of two pioneering studies reporting in-situ measurements of W speciation under hydrothermal conditions. First, Wesolowski et al. (1984) provided the results of potentiometric titrations of tungstate-bearing solution in the range 100-300 °C and revealed that polytungstates ($H_{10}(WO_4)_6^{2-}$, $H_7(WO_4)_6^{5-}$, $H_{18}(WO_4)_{12}^{6-}$) dominate the speciation in the 10^{-2} $mol{\cdot}kg_{H2O}^{-1}$ solution below pH 5. This later total W concentration (i.e. about 2000 ppm) is already relatively high compared to natural ore-forming fluids. However, it is not irrelevant as W concentrations > 1000 ppm are frequently reported from in-situ

analysis of fluid inclusions associated with W-ore deposits (Korges et al., 2018; Beuchat et al., 2004). At lower W concentrations, the monomers (HWO_4^- and WO_4^{2-}) become increasingly stable, but at least one polymer ($H_{10}(WO_4)_6^{2-}$) remains predominant at pH below 3 up to 350 °C. Second, thanks to in-situ Raman spectroscopy, Bilal et al. (1986) showed two stable polymeric W-species, $W_{10}O_{32}^{4-}$ and $H_3W_{12}O_{40}^{5-}$, that dominate the W speciation at T up to 200 °C under acidic and circum-neutral conditions (W concentration in their experiments was not provided but it is supposedly $\geqslant$ 0.01 mol.kg_{H2O}^{-1}). They did not succeed in detecting the presence of HWO_4^- over the 3-9 pH range and concluded that the polymerization degree increases with increasing temperature and pressure. Recently, Wang et al. (2020a, 2020b) performed an in-situ Raman spectroscopic investigation of the hydrothermal speciation of tungsten under moderately acidic (pH > 4 at room T) to alkaline conditions and W concentrations down to 0.005 mol.kg_{H2O}^{-1}. Although these authors unambiguously detected the presence of polymeric species of W under somewhat acidic conditions, at least at T up to 300 °C, they ignored them in their thermodynamic modelling. Interestingly, as mentioned above, the W polymers supposed to be present at elevated temperature do not correspond to those well identified at ambient conditions such as paratungstate A ($W_7O_{24}^{6-}$, with a C_{2v} symmetry), paratungstate B ($H_2W_{12}O_{42}^{10-}$, with a C_1 symmetry) or α-metatungstate ($H_2W_{12}O_{40}^{6-}$, with a Keggin structure). To our knowledge, these four studies (Wesolowski et al., 1984; Bilal et al., 1986; Wang et al., 2020a, 2020b) are the only ones that document W speciation under hydrothermal conditions using in-situ techniques. They demonstrate that polymeric W-species may remain in solution at elevated T-P and circumneutral to acidic pH conditions and display significant disagreements regarding the polymer nature and their respective stability.

To fill this gap, we used quantitative in-situ Raman spectroscopy on W-bearing aqueous solutions at T up to 400 °C to determine the identity, stability, concentrations and thermodynamic properties of dissolved tungsten species in the Na-WO_4-Cl-CO_2-H_2O system over a wide range of pH and tungstate/chloride concentrations. This new data allows for the first-time quantitative predictions of the abundance of W polymers in geological fluids and the evaluation of their role on W transport and deposition in ore deposits.

2. Methods

2.1. Experiments

Tungsten salts - sodium tungstate dihydrate (Na_2WO_4, $2H_2O$, ®Sigma-Aldrich) or sodium metatungstate hydrate ($Na_6W_{12}O_{39}H_2O$, ®Sigma-Aldrich) - were dissolved in milli-Q water (resistivity of 18.2 MΩ·cm at 25 °C) to prepare the W-bearing aqueous solution. The initial total W concentration was generally set to 0.1 m (mol.kg_{H2O}^{-1}), but some experiments were conducted at lower W concentrations (0.01 and 0.05 m). The effect of pH, chlorinity and dissolved carbonate/bicarbonate concentration on W speciation was studied by mixing a known amount of the following reagents: NaCl, NaOH, HCl, HCOOH, CH_3COOH, NH_4Cl, CH_3COONa, $NaHCO_3$, Na_2CO_3, and CO_2 (see below for the loading procedure of CO_2 gas). A summary of each solution with the values of parameters used is given in Table 1. All solutions were prepared a minimum 12 hours before the experiments and kept at room T all along this period. The solutions analyzed 12 to 24 hours after being prepared are noted hereafter “fresh”, compared to those measured more than one month later, labelled “aged”. pH was measured at room temperature using a glass combined electrode and calculated at elevated T using the HCh software package (Shvarov, 2008).

Table 1. List of hydrothermal solutions. Concentrations are expressed in molality ($mol \cdot kg_{H2O}^{-1}$)

# SOL	$pH_{25°C}$	W from $Na_6W_{12}O_{39} \cdot H_2O$	W from $Na_2WO_4 \cdot 2H_2O$	HCl	NaCl	NaOH	$NaHCO_3$	Na_2CO_3	CH_3COOH	HCOOH	CH_3COONa	CO_2 (mbar)	NH_4Cl
1	1.10	0.1		0.1									
2	6.87		0.1	0.1									
2.2	7.06		0.2	0.1									
3	0.15	0.1		1.0									
5	5.60	0.1			0.1								
6	10.58		0.1		0.1								
8	9.56		0.1		3.6								
9	10.06	0.1				0.1							
10	13.02		0.1			0.1							
10.1	13.03		0.01			0.1							
10.2	12.94		0.05			0.1							
10.3	12.98		0.2			0.1							
11	8.90		0.1				1.1						
11.1	7.50		0.1				0.1						
11.2	8.32		0.05				0.1						
11.3	8.31	0.05					0.1						
12	7.2		0.1									151	
12.1	7.2	0.1										199	
13	11.85		0.1					1.2					
R1	4.00		0.1						0.5				
R1.2	2.75	0.1							0.5				
R2	3.00		0.1							0.5			
R2.2	2.00	0.1								0.5			
R3	9.00		0.1								0.5		
R3.2	7.80	0.1									0.5		
N1	7.12		0.1										1.05

2.2. Spectroscopic cell and Raman data acquisition

Solutions must be contained in a material that satisfies several constraints to obtain high-quality Raman spectra. First, the cell material must have sufficient mechanical resistance at the experimental T-P conditions. Second, it must be transparent in the visible spectral region, and it must not induce fluorescence. Third, the cell material must be chemically inert when in contact with aqueous solutions and must not generate catalytic or redox processes. Fused silica capillary capsules (FSCC) satisfy all these requirements (Chou et al., 2008; Caumon et al., 2013; Dargent et al., 2013; Truche et al., 2014). The capillaries were purchased from Polymicro Technologies, LCC, with an internal diameter of 100 µm and an external diameter of 320 µm. The sample loading procedure includes the following steps: (1) the silica tube was sealed at one extremity using an H_2-O_2 micro torch (Elmaflame), (2) the solution (Table 1) was loaded from the open end of the

tube and centrifuged towards the closed end at 12000 rpm, (3) the open end of the tube was connected to a vacuum line, then immersed into liquid nitrogen to freeze the solution, and the atmosphere above the frozen solution was evacuated, (4) CO_2 gas (when needed) was loaded cryogenically, and (5) the open end of the capillary was sealed using a hydrogen flame, while the closed end was kept frozen in liquid nitrogen under vacuum. The pressure of CO_2 loaded cryogenically is estimated to be 10 bar at 20 °C. The partial gas pressure was calculated from the pressure drop in the source reservoir. The method accuracy was considered to be within 20 %, based on volume errors and pressure uncertainty.

A heating-stage dedicated to capillary heating at saturated vapour pressure (®CAP-500 Linkam) was used to reach the experimental T, with an accuracy of ±0.1 °C in the range of 20 – 400 °C. The heating stage was coupled with a Raman spectrometer (Labram HR, ®Jobin-Yvon, Horiba) and an optical microscope (®Olympus). The best compromise combining the highest intensity of the ν_1 Raman band of the tungstate ion and the best rejection of silica-glass spectrum was obtained using a 20× magnification and a 500 µm diameter for the confocal hole. Using a grating of 1800 grooves per mm, the 800 mm focal distance of the spectrometer and the 100 µm slit width, a spectral resolution of 0.5 cm^{-1} is obtained. The 514.532 nm line of an Ar^+ laser (spectra physics, ®Newport Corporation) was used, with a laser power of 70 mW. The spectra were collected in the spectral interval between 150 cm^{-1} and 4500 cm^{-1}, after 60 s acquisition time per spectral window and four accumulations. The measurements were performed first at room temperature (22±1 °C, without considering laser heating) and from 100 °C, up to 400 °C by step of 100 °C at a heating rate of 10°C·min^{-1} for each solution coexisting with a vapour phase below the critical point.

2.3. Fitting procedure of the Raman spectra

We used commercial software ®LabSpec 5.64.15 and ®OriginPro9 to determine peak position, intensity, area, and shape factor for each component in the liquid phase. After baseline subtraction, the decomposition was made using a pseudo-Voigt function (a linear combination of Gaussian and Lorentzian functions). Dissolved W species have Raman bands localized in the 860-1010 cm^{-1} wavenumbers region. The wavenumbers were constrained before the fitting calculation at the maximum intensity of the different band components of the W species in the 860-1010 cm^{-1} region. After baseline correction, each Raman peak was integrated (A_i) and normalized to the area of the O–H bending band of water (A_{H2O}) between 1450 and 1850 cm^{-1}. Fig. 1 displays typical raw Raman spectra of W-bearing solutions obtained at T ranging from 25 to 400 °C. A zoom on the wavenumber domain corresponding to the symmetric stretching (W=O) vibrations is also shown in this figure.

The tungstate (WO_4^{2-}, hereafter noted "B") concentration was calculated using calibration equations established from measurements in four strongly alkaline solutions having total W concentrations ranging from 0.01 to 0.2 m. In the 860-1010 cm^{-1} spectral region, where the presence of W species may be identified, the Raman spectra collected with these standard solutions display a single symmetric band at around 927 cm^{-1}, without any additional features that might suggest the presence of other complexes (Figs. 2A, B).

We used a linear relationship (Eq. 1) between the volumetric concentration of tungstate (C_i, mol·L^{-1}) and its H_2O-normalized Raman band area (A_i) to determine the calibration coefficient (K_i, see Appendix A, Table A.1, Figs. A1.1, .2) of this species at a given T (Figs. 2C, D).

$$C_i = K_i(T) \times A_i \quad (1)$$

The calibration coefficient (K_i) depends on the Raman cross-section of the considered band and the spectrometer response. The tungstate volumetric concentration at each investigated T was previously derived according to Eq. 2 (Appendix B, Tables B.1-10):

$$C_i = (\rho_{fluid}/F) \times m_i \quad (2)$$

where m_i is the molality of tungstate ($mol \cdot kg_{H2O}^{-1}$), F the molinity to molality conversion factor F= 1000/(1000-b) where b is the mass in grams of total dissolved solutes per 1 kg of liquid, and ρ_{fluid} the density ($g \cdot cm^{-3}$) of aqueous solution at a given T and vapour saturation pressure. The density was measured at 25 °C and 1 bar by weighing 1 ml of each solution. The knowledge of the density at high temperature necessitated computational models because we had no control over volumetric variations of the solution inside the FSCC during heating. For this purpose, we compared the soWat model (Driesner and Heinrich, 2007; Driesner, 2007) with the AqSo-NaCl model (Bakker, 2018). These two models require (i) the calculation of NaCl mole fraction, according to Eq. 3:

$$xNaCl = mol_{eqNaCl}/[m_{eqNaC}+(1000-b)/u_{H2O}] \quad (3)$$

where b is the mass in grams of total dissolved solutes per 1 kg of liquid and u_{H2O} is the molecular mass of water, and (ii) the pressure value of the solution at each investigated T: 1, 0.9, 15, 85.83 and 220 bar for T = 25, 100, 200, 300 and 400 °C, respectively. Both methods gave the same results at the second decimal level (Appendix B, Tables B.1-10).

The obtained calibration coefficients for species B at T ranging from 25 to 400 °C (Figs. 2C, D) allows us to quantify its concentration in all solutions and estimate the concentration of the other W species thanks to the following procedure. First, in all the collected Raman spectra, we identified those displaying only one Raman band in addition to that of tungstate (at 927 cm^{-1}) in the 860-1010 cm^{-1} spectral region. This configuration existed only under circum-neutral to mid-alkaline conditions - the C species being the only secondary Raman band contribution. Second, we derived the W concentration belonging to the C species by subtracting the previously calculated tungstate concentration (B-species) from the total W concentration of the solution. Third, we inferred the calibration coefficient (k_c) for the C species at T ranging from 25 to 400 °C and calculated the W concentration of C species in all our solutions. Finally, we repeated this step-by-step procedure for Raman spectra displaying three and eventually four Raman bands in the 860 - 1010 cm^{-1} spectral region. Of course, uncertainty increased over the curse of this approach because of growing cumulative errors and because some calibration lines were poorly constrained (Appendix C - Tables C.1-3).

3. Results

A total of 5 different Raman bands were detected in the 860 - 1010 cm^{-1} spectral region, which corresponds to the symmetric stretching (W=O) vibration domain. This latter domain is overlapped by the asymmetric stretching (W=O) vibration domain ranging from 825 to 930 cm^{-1}. These Raman bands are identified with alphabetic letters (A, B, C, D, E) and ranked by increasing wavenumbers in the following sections. The corresponding W-species include simple dissolved ions, clusters and polyanion species, like heteropoly acids with kegging structures known as heteropolytungstates. We discuss their respective Raman band attribution in section 4.1.

3.1. Effect of temperature and pH on W speciation

Fig. 3 shows four series of Raman spectra corresponding to four different W-bearing aqueous solutions collected at different pH conditions and T ranging from 25 to 400 °C. Under strongly alkaline conditions (Fig. 3A), only one single Raman band exists in the 860 - 1010 cm^{-1} spectral region at each investigated T. This band noted "B" is identified by its intense and sharp features at ~ 923 cm^{-1} at 25 °C, which slightly shifts toward lower frequencies with increasing T. Under acidic to circum-neutral conditions, W speciation is far more complex, with up to five well-identified Raman bands coexisting over the investigated T range. The relative evolution of the area of these bands reflects the evolution of the speciation of tungsten.

The Raman band noted "A" is characterized by a broad and weakly intense peak at ~ 894 cm^{-1}. At room T, this band exists in solution from strongly acidic to neutral conditions (Fig. 3B-D), and its area normalized to the water bending band slightly increases over the 1.1 to 6.9 pH range. The intensity of this "A" band decreases with T and vanishes at T above 200 °C. The Raman band noted "B", previously identified under alkaline conditions, exists over all the investigated pH and T ranges. Still, its intensity decreases abruptly under circum-neutral pH conditions and remains very low under acidic conditions. The Raman band noted "C" is identified by an intense and sharp peak at ~ 960 cm^{-1} at room temperature. Its intensity is maximum under circum-neutral conditions, but it decreases rapidly with increasing pH and disappears at a pH around 11. However, the intensity of this "C" band only slightly decreases under acidic conditions and remains significant even at a pH below 1 at room T. A slight wavenumber shift toward lower values with increasing T is also observed for this band. The Raman band noted "D" appears at a pH below 7 at room temperature. It is characterized by an intense and sharp peak at ~ 970 cm^{-1}, downshifting toward slightly lower wavenumbers as T increases. This band is the most intense of all at pH values below 7 and a temperature of 25 °C. It remains detectable in solution at T up to 400 °C, but a fifth band (noted "E") progressively replaced it at T ≥ 200 °C. This latter band is well identified by a sharp and intense peak at ~ 988 cm^{-1} at 200 °C, downshifting to ~ 983 cm^{-1} at 400 °C. At a pH below 2 and T > 200 °C, precipitation occurs, and no more dissolved W-species remains detectable.

3.2. Stability and reversible formation of polytungstates

The question of the stability and reversibility of the previously described W speciation was addressed in three different ways: 1) by comparing Raman spectra acquired immediately after heating the capillary at 200, 300, and 400 °C with those obtained at the same temperature after forty-eight hours of pre-heating at 350 °C, 2) by performing heating and cooling cycles, and 3) by measuring W speciation at 25 °C two months after having heated the capillary to 400 °C and by comparing the obtained Raman spectra with both fresh and aged (after six months) unheated solutions.

Fig. 4 shows one example of these tests performed on a capillary containing a solution at 0.1 m total W concentration from Na_2WO_4 and 0.5 m acetic acid (#R1), having a pH = 4 at 25 °C, and thus being demonstrative of the evolution of the five previously described Raman bands. The comparison of the Raman spectra obtained at 200, 300, and 400 °C immediately after loading the capillary (Fig. 4A, lower part) and after 48 hours of pre-heating at 350 °C (Fig. 4B) are perfectly identical in terms of peak feature (Full Width at Half Maximum FWHM and Gravity Center of the band) and peak intensities (Maximum Height), when normalized to water bending (see Appendix D – Table D). The W speciation is also fully reversible upon heating-cooling cycles over the 200 - 400 °C T range. The D and E Raman bands observed at 200 °C and 300 °C disappear in favour of species C at 400 °C. These two first tests demonstrate that the four

Raman bands B, C, D and E belong to four different W species. They also show that these four species are stable and that ~~the~~ equilibrium is achieved within minutes under hydrothermal conditions. However, the third test, which consists of comparing Raman spectra obtained at room T with i) freshly prepared, ii) aged, and iii) heated up to 400 °C solutions, shows a different picture (Fig. 4A). In particular, ~~the~~ species E, not present in the fresh solution, remains abundant in the solution immediately or two months after cooling. Species C, which was present in the initial solution, is absent after cooling, and the abundance of species D is different before and after heating/cooling. Note that W speciation at 25 °C in the unheated solution remains nearly identical in the freshly prepared solution and after six months of ageing. This latter comparative test demonstrates that W-speciation does not reflect equilibrium as observed on the initial solution. The freshly-prepared W-bearing solution is in a metastable equilibrium state. Equilibrium would require more than six months to be reached at 25 °C, species E being the thermodynamically stable by-product of the D (and probably C) species decomposition in solution. It should be noted that species B, C, D and E are present in the system even at ten times lower W-concentration (0.01 m total W concentration; Fig. 5).

3.3. Effect of carbonate and chloride ligands

The effect of carbonate on W-speciation was studied using three contrasting carbonate-bearing systems, where either CO_2(aq) (solution #12, $pH_{25°C}$ = 7.2), HCO_3^- (solution #11, $pH_{25°C}$ = 8.3), or CO_3^{2-} (solution #13, $pH_{25°C}$ = 11.9) were the dominant dissolved carbonate species. At room T, the in-situ pH value of the W-bearing solution (0.1 m Na_2WO_4) in equilibrium with 0.15 bar CO_2(g) was estimated using HCh software package (Shvarov, 2015), based on the relative abundance of HCO_3^- and CO_2(aq). The Raman spectra shown in Fig. 6 are strictly identical to those obtained under similar pH and T conditions without carbonate (see Fig. 3). Thus, the presence of dissolved carbonate in a substantial amount (> 0.1 m) has no effect on W speciation over the $6 < pH < 12$ and $25 \leq T \leq 400$ °C ranges.

The effect of chloride on W speciation was examined through three solutions in the presence of 0.1 to 3.6 m NaCl. Fig. 7 shows the Raman spectra collected for two different W-bearing solutions containing 3.5 m NaCl, at different $pH_{25°C}$ values: 5.3 and 9.6, respectively. In both systems, chloride complexation with dissolved W species does not occur, as no new species are detected in the solution other than those already described. Under slightly acidic condition (Fig. 7A), W speciation remain identical to the one measured in solution #5 (low chloride content and $pH_{25°C}$ = 5.6), up to 300 °C. At high salinity (Fig. 7), the presence of species "C" seems to be promoted in comparison with the chloride-low solutions conducted under similar pH conditions (i.e. solutions #5 and #6; Fig. 3).

4. Discussion

4.1. Identification of W-species

Among the five previously detected Raman bands, only the one at 927 cm^{-1} belonging to species "B", may be assigned with certainty to the ν_s(W=O) symmetric stretching vibration of the WO_4^{2-} anion (Ng and Gulari, 1984; Bilal et al., 1986; Vigasina et al., 2000; Barré et al., 2005; and Redkin and Bondarenko, 2010). Note that the ν_{as}(W=O) asymmetric stretching mode at 834 cm^{-1} and the δ(W=O) bending mode at 326 cm^{-1} of WO_4^{2-} are hindered by the Raman bands of the silica-glass of the FSCC. The other four observed bands (at ~890, 955, 970 and 985 cm^{-1}) are much more difficult to assign to a specific W species as there is no consensus in the literature. However, one crucial finding of this study is that all the detected species under hydrothermal conditions exist in solution at room temperature, even species "E" that forms

upon heating at T ≥ 200°C but remains stable two months after cooling at room temperature. Thus, the observed W-species are not specific to the hydrothermal condition. They must have been described in the plethora of studies dedicated to W speciation at ambient condition.

In an attempt to propose a first comprehensible identification of these W-species, we cross-compare the published Raman spectroscopic studies (Appendix E - Table E.1) with other sources of W speciation data: potentiometric titration, solubility experiments, ultracentrifugation, mass spectrometry, Nuclear Magnetic Resonance (Appendix E - Table E.2), and thermodynamic calculations (Appendix E - Table E.3). This exercise allows us to infer the most probable W species associated with each Raman peak previously observed. At W concentration above 0.01 m, there is a large consensus in the literature (see recent review by Gumerova and Rompel, 2020) that when an aqueous solution of tungstate is acidified, condensation reactions lead to the formation of polytungstates.

Species "A" - Raman band at 888-892 cm^{-1}. The morphology of this Raman band is very different from the others: low intensity and very large full-width at half maximum (averaged FWHM are 24, 18 and 14 cm^{-1} at 25 °C, 100 °C and 200 °C, respectively). This Raman band is only detected at T ≤ 200 °C and pH < 8. It is always associated with the presence of the "D" and/or "C" bands, and its normalized intensity varies accordingly with these latter bands. The Raman spectra of Keggin hetero-polytungstate anions exhibit bands between 950 and 1015 cm^{-1} (ν_s(W=O) symmetric stretching mode) and 825-930 cm^{-1} (ν_{as}(W=O) asymmetric stretching mode) as well as bands at lower wavenumbers arising from the bridging W-O-W bonds (Ross-Medgaarden and Wachs, 2007). Thus, this later behaviour leaves us thinking that the "A" band corresponds to the weak asymmetric stretching (W=O) vibrational mode of species "D" and "C".

Species "C" – Raman band at 950-960 cm^{-1}. This band is sharp and intense. It is located next to WO_4^{2-} (species "B"), with a slight upshift in wavenumbers. It exists at all investigated T and $pH_{25°C}$ < 10.5. Its maximum intensity is reached at $pH_{25°C}$ ~ 7 and room T. The species "C" may coexist alone with WO_4^{2-} at 7< $pH_{25°C}$ <10.5 and at T up to 400 °C (Fig. 3C). At T > 300°C, it forms at the expense of species E (and D to a lesser extent) and its formation at elevated T is fully reversible upon cooling. Redkin and Bondarenko (2010) assumed this band to be related to the vibration of $[HW_6O_{21}]^{5-}$, by analogy with thermodynamic simulations relying on data reported by Baes and Mesmer (1976) and Wesolowski et al. (1984). In their extensive potentiometric investigation of W(VI) speciation at 300 °C, Wesolowski et al. (1984) considered several criteria to select three speciation schemes compatible with their data. Among the three speciation schemes, two including $[W_7O_{24}]^{6-}$ were proposed, but slight preference was given to that comprising the two hexamers $[HW_6O_{21}]^{5-}$and $[W_6O_{19}]^{2-}$ in addition to monomers and the dodecamer $[H_2W_{12}O_{40}]^{6-}$. The inclusion of hexameric or heptameric species in their speciation scheme under weakly acidic conditions is debatable. Indeed, since the pioneering work of Jander et al. (1929), the hexameric anion has been included in nearly all speciation models. However, such a choice was unequivocally removed by the combined results of NMR (Maksimovskaya and Burtseva, 1985; Hasting and Howarth, 1992), potentiometric (Cruywagen and Van Der Merwe, 1987), cyclic voltammetric (Himeno et al., 2000), and Raman (Fuchs and Flindt, 1979; Himeno et al., 2000) studies. All these works favour the existence and stability of $[W_7O_{24}]^{6-}$ in this pH domain. This species displays a strong ν_s(W=O) symmetric stretching Raman band at ~ 953 cm^{-1} at room temperature (Fuchs and Flindt, 1979; Himeno et al., 2000; Weiner et al., 2005). A comparison of the Raman spectrum of $[W_7O_{24}]^{6-}$ in the solid-state (isolated as a piperidinium salt) and a freshly acidified tungstate solution led to the identification of $[W_7O_{24}]^{6-}$ in solution (Fuchs and Flindt, 1979). A remarkable similarity was noted between the infrared spectra of heptamolybdate salts and the spectra of $[W_7O_{24}]^{6-}$ in solution (Pope, 1983). Maksimovskaya and Burtseva (1985), thanks to a ^{17}O and ^{183}W NMR investigation of tungstate solutions, showed the presence of both

$[W_7O_{24}]^{6-}$ and $[H_2W_{12}O_{42}]^{10-}$. The equilibrium concentrations between these two species depends on temperature and total W concentration. Despite all these lines of evidence, Wang et al. (2020a) recently assigned this Raman band to HWO_4^-, to comply with the thermodynamic predictions made by Wesolowsky et al. (1984) or Wood and Samson (2000). We disagree with this choice, even if we recognize that this band assignment is tempting, mainly because it satisfies the classical view of W speciation at elevated temperature and the fact that neutral or weakly charged species are favoured under hydrothermal conditions due to the decrease of the dielectric constant of water (e.g. Crerar et al. 1985; Brimhall and Crerar, 1987). Because of polynuclear W ions, the HWO_4^- was never observed by spectroscopic techniques, even at very high dilution (Cruywagen, 1999). The Raman band at 950-960 cm^{-1} is kept at room T over a wide pH range (from pH = 1 to nearly 10), and its main features (i.e. position and FWHM) do not change with T. This key observation contradicts the existence of HWO_4^-, a species never reported in such conditions. Therefore, we assigned the Raman band at ~953 cm^{-1} to $[W_7O_{24}]^{6-}$ (paratungstate-A).

Species "D" – Raman band at 970-979 cm^{-1}. At room temperature and a pH < 6, this band is the most intense of all. Its intensity strongly decreases at T ≥ 200 °C but remains detectable up to 400 °C under acidic conditions (pH < 5). The disappearance of this band at elevated T is not reversible upon cooling (Fig. 4). Therefore, the species "D" is metastable. Bilal et al. (1986) assigned this band to the $[W_{10}O_{32}]^{4-}$ species (tungstate-Y) in their Raman spectra recorded at 150°C, 1 kbar and $pH_{150°C}$ = 6. These authors also observed the complete disappearance of this band at T = 200 °C. This behaviour is in good agreement with our observations. Tungstate-Y is known to be kinetically unstable in aqueous solutions (Gumerova and Rompel, 2020). Upon prolonged heating at 80 °C, it yields the thermodynamically stable true α-metatungstate α-$[H_2W_{12}O_{40}]^{6-}$ (Hasting and Howarth, 1992; Himeno and Kitazumi, 2003). Thus, we assigned the Raman band at 970-979 cm^{-1} to $[W_{10}O_{32}]^{4-}$ (tungstate-Y).

Species "E" – Raman band at 983-995 cm^{-1}. This band is very sharp (averaged FWHM are 7, 6, and 2 cm^{-1} at 200, 300, and 400 °C, respectively) and intense. It only appears at a pH ≤ 7 and T ≥ 200 °C upon heating. It forms at the expense of species "D". The behaviour of the species corresponding to this band is surprising since its formation is reversible upon heating and cooling in the 200 – 400 °C T range. Once formed, it remains stable at room temperature even after two months (Fig. 4). This band was assigned to the $[W_{10}O_{32}]^{4-}$ by Himeno et al. (2000) in their Raman spectra obtained at room T and a pH < 4, without heating. They observed the band disappearance upon increasing the pH above 3 or after heating at 80 °C for three days. This behaviour is inconsistent with our observations: species E forms upon heating preferentially under slightly acidic conditions. Thus, we rule out the possibility for $[W_{10}O_{32}]^{4-}$ to belong to this Raman band at 983-995 cm^{-1}. This band was assigned to $[H_3W_{12}O_{40}]^{5-}$ by Bilal et al. (1986) in their spectra recorded at 150 °C, 1 kbar and $pH_{150°C}$ = 6. These authors also observed that this complex is the only stable polymeric species at a pH < 5, T = 200 °C and P = 1 kbar. Again, this observation is in excellent agreement with our measurements. Other minor species (mainly B and D) may be attributed to lower pressure (vapour saturation pressure) or a better sensitivity of our spectrometer. Wang et al. (2020a) also detected this band in their experiments performed from 0.03 to 0.1 mol kg_{H2O}^{-1} of total W concentration in the presence of CO_2. Still, they did not assign it to a particular polymeric species. In their thorough and comprehensive NMR spectroscopy study (^{183}W, ^{17}O and ^{1}H) of tungstate solution in the pH range 1.5 to 8, Hasting and Howarth (1992) gave an in-depth perspective on the formation of W species in solution based on poly-oxoanions already characterized in the solid-state. The $[H_3W_{12}O_{40}]^{5-}$ polyanions is a protonated form of paratungtate-B ($[H_2W_{12}O_{42}]^{10-}$) that forms at pH < 2. This description does not correspond to our observations because species E appears at T > 100 °C and slightly acidic conditions. Thus, $[H_3W_{12}O_{40}]^{5-}$ and $[W_{10}O_{32}]^{4-}$ complexes cannot be assigned to the Raman band at 983-995 cm^{-1}. Instead, the well-known behaviour of α-metatungstate (α-$[H_2W_{12}O_{40}]^{6-}$) which is the

dominant and thermodynamically stable W-species that forms upon prolonged heating (70 °C) below pH 6 (Hasting and Howarth, 1992; Himeno et al., 2000, Himeno et Kitazumi, 2003) satisfies all our observations. Therefore, we assigned the Raman band at 983-995 cm^{-1} to α-$[H_2W_{12}O_{40}]^{6-}$ (α-metatungstate).

Sodiated tungstate species were never reported in the literature (see review by Gumerova and Rompel, 2020), and a recent (preliminary) XAS investigation under hydrothermal conditions tends to confirm the absence of sodiation (Klemme et al., 2021). Salts containing fragments of heptatungstate structure, $Na_5[H_3W_6O_{22}]$ (Hartl et al., 1993), were isolated from concentrated weakly acidic aqueous solutions, but there is no evidence that this anion is stable in solution. The fact that protonated and non-protonated polytungstate species may coexist simultaneously and non-protonated species may even dominate W speciation under very acidic conditions relies on experimental data reported by numerous studies (see Gumerova and Rompel, 2020 for a review). Part of this observation may be explained by the enthalpy factor of the condensation process and by the metastability of some anions. However, DFT calculations are definitively needed to solve this critical question.

4.2. Tungsten speciation

Based on our calibration procedure, we were able to derive the concentration of WO_4^{2-} and to estimate step by step the concentration of the three other identified species, namely $[W_7O_{24}]^{6-}$, $[W_{10}O_{32}]^{4-}$, and α-$[H_2W_{12}O_{40}]^{6-}$ in all our solutions at each temperature up to 400 °C. The obtained calibration coefficient (K_T) values are within the 0.01 to 0.2 $mol.L^{-1}$ range. Surprisingly, the tungsten polymerization does not significantly affect the value of the Raman scattering coefficients. These coefficients tend to decrease with temperature starting from about 0.15 $mol.L^{-1}$ at 25 °C and decreasing abruptly to 0.02 – 0.04 $mol.L^{-1}$ at T > 200 °C. Only the calibration coefficient of the $[W_7O_{24}]^{6-}$ species displays a significantly different behaviour, with a slight increase with T from 0.15 to 0.2 $mol.L^{-1}$ over the 25 – 400 °C T range. The solution pH was measured at room temperature and then calculated at elevated temperature using the the HCh software package (Shvarov, 2008). This approach is relatively safe under extreme pH conditions (pH < 3 or pH >10) or in the presence of concentrated pH buffers (acetic acid, formic acid, carbonate/bicarbonate solutions) because the evolving tungsten speciation weakly impacts H^+ activity. However, for a small number of solutions (e.g. sol.#2, #2.2 and #5) where the circum-neutral pH conditions measured at ambient conditions were not buffered, our calculations were made for the indicative purpose as there is no thermodynamic data available a priori for the observed complex at elevated temperature. The resulting tungsten speciation as a function of pH is shown in Fig. 8 at 25, 100, 200, and 300 °C.

The WO_4^{2-} anion is the predominant species at a pH above 7.5 and T = 25 °C. Its predominance domain is slightly shifted toward a lower pH value with increasing temperature. Interestingly, we detected and quantified the presence of WO_4^{2-} even under strongly acidic conditions, where it still represents between 5 to 10 % of the total dissolved W concentration. The $[W_7O_{24}]^{6-}$ polyanion is the predominant species under circum-neutral conditions (6 < pH < 7) at T up to 100 °C. This latter species still represents an essential contribution to the W speciation (20 to 40 %) at lower pH. At higher T, its concentration in solution drastically decreases, and it only represents 10 to 20 % of the total dissolved W concentration. The $[W_{10}O_{32}]^{4-}$ polyanion, which is metastable, dominates the W speciation at pH < 5 and T up to 200 °C upon heating. Under these conditions, its concentration represents 40 to 80 % of the total W speciation. Upon further heating $[W_{10}O_{32}]^{4-}$ progressively disappears in favour of α-$[H_2W_{12}O_{40}]^{6-}$. The disappearance of $[W_{10}O_{32}]^{4-}$ is not reversible upon cooling. Finally, the α-$[H_2W_{12}O_{40}]^{6-}$ polyanion is the most abundant and stable species at pH < 6 and T ≥ 300 °C. Once formed, α-$[H_2W_{12}O_{40}]^{6-}$ remains in solution upon cooling, which is not the case for $[W_{10}O_{32}]^{4-}$.

4.3. Thermodynamic calculations

Raman spectroscopy data on W speciation obtained in this study were used to calculate the stability constants of W polymers. The following reactions describe their formation from WO_4^{2-}:

$$7WO_4^{2-} + 8H^+ = W_7O_{24}^{6-} + 4H_2O \quad (1)$$

$$10WO_4^{2-} + 16H^+ = W_{10}O_{32}^{4-} \quad (2)$$

$$12WO_4^{2-} + 18H^+ = H_2W_{12}O_{40}^{6-} + 8H_2O \quad (3)$$

Besides, the following pH-independent reactions can be written:

$$4WO_4^{2-} + W_{10}O_{32}^{4-} = 2W_7O_{24}^{6-} \quad (4)$$

$$21WO_4^{2-} + 24W_{10}O_{32}^{4-} + 20H_2O = 20H_2W_{12}O_{40}^{6-} + 3W_7O_{24}^{6-} \quad (5)$$

The most important W polymers (~50% of dissolved W) coexisting with high amounts of WO_4^{2-} (~50% of dissolved W) under our experimental conditions are $[W_7O_{24}]^{6-}$ at 25 – 100 °C and α-$[H_2W_{12}O_{40}]^{6-}$ at 200 - 300 °C. The experimentally determined concentrations (in mol·kg_{H2O}^{-1}) of these polymers and WO_4^{2-} together with the corresponding estimated pH values were used to calculate the apparent constants for the reactions 1 and 3 according to:

$$log_{10}K_m(1) = log\frac{m(W_7O_{24}^{6-})}{[m(WO_4^{2-})]^7} + 8pH \quad (6)$$

$$log_{10}K_m(3) = log\frac{m(H_2W_{12}O_{40}^{6-})}{[m(WO_4^{2-})]^{12}} + 18pH \quad (7)$$

At 25°C and pH above 6.5, a good consistency between the pH and WO_4^{2-} and $[W_7O_{24}]^{6-}$ concentrations were found for all solutions except that under high NaCl concentration (3.6 m NaCl). We expect this to be caused by the increased uncertainty in classical pH measurements at high NaCl concentrations. Thus, this point was excluded from the analyses. For the other experiments at pH 6.5 - 8.5, the pH values within ± 0.3 uncertainty were described by the apparent constant $\log_{10}K_m(1)$ value 67.1 ± 1.5 calculated according to equation (6). At pH below 6.5, the equilibrium between WO_4^{2-} and $[W_7O_{24}]^{6-}$ does not seem to be reached, i.e. there is no stable relationship between the pH value and WO_4^{2-} and $[W_7O_{24}]^{6-}$ concentrations. The pH-independent reaction (4) was calculated as:

$$log_{10}K_m(4) = log\frac{[m(W_7O_{24}^{6-})]^2}{[m(WO_4^{2-})]^4 \cdot m(W_{10}O_{32}^{4-})} \quad (8)$$

The apparent constant $\log K_m(4)$ was found to be 5.4 ± 1.0 for all solutions at 25 °C. A similar analysis of W polymers formation was done at 100 °C. The corresponding constant is given in Table 2.

At 200 - 300 °C, α-$[H_2W_{12}O_{40}]^{6-}$ and WO_4^{2-} distribution in experimental solution as a function of pH can be described by the apparent constants given in Table 2.

Table 2. Apparent constants determined in this study

Reaction		T	$logK_m$	$I_{m(T)}$	pH_T
$7WO_4^{2-} + 8H^+ = W_7O_{24}^{6-} + 4H_2O$	(1)	25°	67.1 ± 1.5	0.3-0.7	≥ 6.5
		100°C	65.1 ± 1.0	0.3-0.7	≥ 6.5
$4WO_4^{2-} + W_{10}O_{32}^{4-} = 2W_7O_{24}^{6-}$	(4)	25°C	5.4 ± 1.0	0.3-1.2	0.1-5.6
		100°C	5.3 ± 1.2	0.3-1.2	0.1-5.6
$12WO_4^{2-} + 18H^+ = H_2W_{12}O_{40}^{6-} + 8H_2O$	(3)	200°C	116.0 ± 3.5	0.3-0.8	4.5-6.0
		300°C	116.0 ± 1.5	0.3-0.8	4.5-6.0

The correction to the ionic strength is required to calculate the constants at infinite dilution. For this correction, the extended Debye-Hückel equation was applied:

$$log_{10}\gamma_i = -z^2 D = -z^2 \frac{A \cdot \sqrt{I_m}}{1 + B \cdot a \cdot \sqrt{I_m}} \quad (9)$$

where D is the Debye-Hückel term with A and B parameters which are constant at a given temperature (Appendix F, Table F.1.), and I_m is the ionic strength, calculated as

$$I_m = 0.5 \cdot \sum_{i=1}^{n} m_i \cdot z_i^2 \quad (10)$$

where m_i and z_i are a concentration (in mol·kg$_{H2O}^{-1}$) and a charge of aqueous species, respectively. The ionic strength was calculated considering the experimental data on W polymer concentrations and assuming all other ions as dissociated. Rather high uncertainties in the pH at elevated temperatures, species concentrations, and ionic strength calculations, together with the use of multiple electrolytes, imply very high uncertainties in activity coefficient calculations. Thus, applying more accurate models of ionic strength correction (e.g. specific ion interaction model or Pitzer model) is meaningless for this study. The extended Debye-Hückel theoretical approach (equation 9) was the most suitable. Constants given in Table 3 were calculated from the apparent constants (Table 2) according to:

$$log_{10}K^0(1) = log\frac{m(W_7O_{24}^{6-})}{[m(WO_4^{2-})]^7} + 8pH - 8D \quad (11)$$

$$log_{10}K^0(3) = log\frac{m(H_2W_{12}O_{40}^{6-})}{[m(WO_4^{2-})]^{12}} + 18pH + 12D \quad (12)$$

The thermodynamic constants of reactions (1) and (2) at 200 – 300 °C were optimized to better reproduce the experimental distribution of W species. The optimized values of thermodynamic constants are given in Table 3.

Table 3. Thermodynamic constants determined in this study

Reaction		T	$log_{10}K^0$
$7WO_4^{2-} + 8H^+ = W_7O_{24}^{6-} + 4H_2O$	(1)	25°C	65.6 ± 1.5
		100°C	62.9 ± 1.5
		300°C	48.8 ± 1.5
$10WO_4^{2-} + 16H^+ = W_{10}O_{32}^{4-}$	(2)	300°C	107.0 ± 1.5*
$12WO_4^{2-} + 18H^+ = H_2W_{12}O_{40}^{6-} + 8H_2O$	(3)	200°C	119.0 ± 3.5
		300°C	119.0 ± 0.5

* this species $[W_{10}O_{32}]^{4-}$ is believed to be metastable (see more discussion in the text).

The value of $log_{10}K(1)$ at T = 25 °C obtained in this study (65.6 ± 1.5) agrees with the literature data (65.19, Cruywagen and Van Der Merwe, 1987). The values of stability constants of W polymers at high temperatures are determined for the first time. In Fig. 9, the speciation of W at 300 °C in 1 m NaCl solution is calculated for Na_2WO_4-HCl-NaOH-H_2O system as a function of pH based on the data reported in Table 3 and by applying equation (9) for the activity coefficient calculation. The polymer $[W_{10}O_{32}]^{4-}$ is expected to be thermodynamically unstable (see section above). The value of $log_{10}K(2)$ given in Table 3 allows estimating some theoretical behaviour of this species under equilibrium. When excluding $[W_{10}O_{32}]^{4-}$, the models predict α-$[H_2W_{12}O_{40}]^{6-}$ as the dominant W species, under low pH. The predominance of W polymers calculated in Fig. 9A does not change when $[W_{10}O_{32}]^{4-}$ is excluded. Thus, our thermodynamic data can be used for modelling hydrothermal transport of W during ore deposit formation.

4.4. Geological implications

The evolution of W-speciation is strongly dependent on temperature and pH. Our experimental study demonstrates that W forms highly-charged polymers up to 400 °C like the para-tungstate A (C species) $(W_7O_{24})^{6-}$, which is stable at all investigated temperatures, and the decatungstate Y (D species) $(W_{10}O_{32})^{4-}$. This latter species is metastable and may be replaced by the dodeca α-metatungstate (E species) $(H_2W_{12}O_{40})^{6-}$ which forms at T ≥ 200 °C. Even if these polymeric species may be considered with caution, they predominate in solution under acidic to circumneutral conditions at temperatures up to 400 °C. The existence of stable, highly-charged polymeric species at temperatures up to 400 °C is a significant discovery as it definitively shifts the long-standing paradigm that only neutral or weakly-charged species predominate under hydrothermal conditions. This is due to the decrease of the dielectric constant of water with´the increasing temperature (Crerar et al., 1985; Mei et al., 2014; Brugger et al., 2016).

Moreover, the W species detected at elevated temperatures also exist at ambient conditions with no new complex or polymers formation. This strong tendency of tungsten to form complexes, like heteropoly-, aquapoly, and isopoly-tungsten compounds, is unique. No other element of the periodic table (not even Mo, the W chemical brother) acts in that way. The contrasting behaviour between W and Mo may be explained by the weakening of bonding of the valence electrons from Mo to W, resulting in the stability increase of the higher oxidation states of W and its tendency to form oxygen compounds having Kegging structure. Mo combines with S to precipitate molybdenite, whereas W still forms oxides like wolframite or scheelite. Equation 13 from Barabanov (1971) shows this strong affinity of W for oxygen in acidic conditions and its gradual weakening with increasing pH values as observed in the present study.

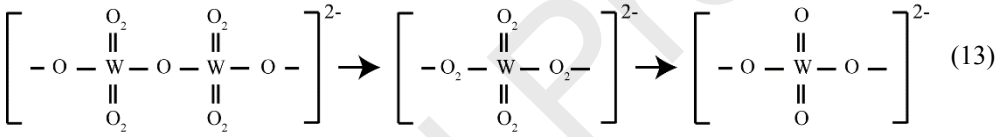

(13)

This new view of W speciation under hydrothermal conditions has significant consequences for W transport and deposition in natural environments by hydrothermal aqueous fluids.

The importance of W polymers in ore-forming hydrothermal fluids was modelled according to thermodynamic data obtained in this study (Table 3) and presented in Fig. 9. The possible input of $HWO_4^-/H_2WO_4^0{}_{(aq)}$ species was calculated according to Wang et al. (2019). The inclusion of this species in the model does not significantly change the speciation of W polymers (see Figs. 9A and 9B). The total W concentration and pH are the main factors controlling the formation of W polymers in Na_2WO_4-NaCl-HCl-NaOH system. The acidic pH and high W contents favor W polymerization (Fig. 9d). Our modeling shows that the concentration of NaCl strongly affects the W speciation due to the high charge of W polymers (see Fig.F.1.3). For example, the role of highly charged species (i.e. W polymers) increases with increasing electrolyte concentration. Moreover, the solubility of W minerals is known to increase with increasing NaCl or KCl concentration (see Redkin and Cygan, 2020 and references cited). In Ca- and Fe-bearing fluids with near-neutral pH, the low solubility of scheelite $CaWO_4$ and ferberite $FeWO_4$ prevents the formation of W polymers. Under more acid conditions, the formation of W polymers would favour high solubility, but under pH below 4.5, the fields of W polymers and WO_3 precipitation overlap (i.e. Fig. 9d). The latter means that the presence of dissolved Ca and Fe in natural fluids does not favour high W concentrations. Tungsten-ore forming fluids may contain more than 1000 ppm W, as recently revealed by fluid inclusion studies (Korges et al., 2018). Such high W concentrations reaching the millimolar range are sufficient to trigger W polymerization, as demonstrated by our in-situ measurements and thermodynamic

calculations (Figs. 5a and 9). Some geological fluids are very rich in W, and a total W concentration of around 2000 ppm is not unrealistic in natural ore-forming fluids (Table 4). We point out here that most fluid inclusion studies were made on quartz that is supposed to be coeval with W-bearing minerals. It implies that the entrapped fluids were partly depleted in W during the ore-forming stage. Despite this phenomenon, these fluids still contain more than 200 ppm of W, and the original W bearing-fluid was probably even richer in W (Naumov et al., 2011; Goldmann et al., 2013; and Hulsbosch et al., 2016). Korges et al. (2018) revealed via in-situ LA-ICP-MS analysis of fluid inclusions from the Sn-W Zinnwald deposit in the Erzgebirge (Germany) that ore-forming fluids contained up to 1000 ppm total W concentration. Beuchat et al. (2004) reported exceptional W enrichment in fluid inclusions from the W-Cu-Zn-Pb San Cristobal district (Peru), with W concentration exceeding 10,000 ppm in quartz from the early W ore deposition stage.

Table 4. W concentrations in natural fluids

METHODOLOGY	SOURCES	W concentrations from literature						
		Beuchat et al., 2004	**Naumov et al., 2011**	**Hulbosch et al., 2016**	**Fusswinkel et al., 2017**	**Zhang et al., 2017**	**Korges et al., 2018**	**Guo et al., 2019**
LA-ICP-MS and Microthermometric FI studies	Wfm-Qtz-Py Stage	100 < ppm < 10000						
Database Review	Magmatic Melts		6.8 ppm (+81 ppm/-6.2 ppm)					
	Mineral-Forming Fluids		30 ppm (+114 ppm/-25 ppm)					
RAMAN on FI Studies	Ms associate with Sch and Frb Tur associate with pegmatite			3 < ppm < 1310				
LA-ICP-MS in FIA	Early Qtz vein				0.03 < µg/g < 9.9			
LA-ICP-MS in FIA	Late Extensional vein				8.24< µg/g <23			
LA-ICP-MS	Two-mica granite					50 < ppm < 70		
LA-ICP-MS in FIA	Wmf-Cst-Qtz						10 < ppm < 10000	
ICP-MS in Active Hydrothermal System	Water samples							0.05 < µg/L < 1103
	Sediments nearby the vents							6.49 < ppm < 536

Abbreviations Legend
Sch = scheelite
Frb = ferbrerite
Tur = tourmaline
Wfm = wolframite
Qtz = quartz
Py = pyrite
Cst = cassiterite
FIA = fluid inclusion assemblage

Usually, fluid inclusions associated with quartz-vein type wolframite deposits are commonly accompanied by the dominant presence of CO_2 (Higgins, 1980; Ball et al., 1985; Wood and Samson, 2000; Rios et al., 2003; Naomov et al., 2011 and Ni et al., 2015). According to Cathelineau et al. (2020), W-ores at Panasqueira W deposit (Portugal) precipitated from low salinity, aqueous-carbonic fluids with CO_2 - CH_4 - N_2 present in the volatile phase. Tungsten does not form complexes with carbonate species over the whole pH and T ranges investigated in the present work. This observation does not preclude an essential role for CO_2/carbonates in the transport and deposition of W: first, the presence of dissolved CO_2 may buffer the pH in the range 5 - 6 and thus favours a W speciation dominated by polymeric species. Second, CO_2/water immiscibility may result in CO_2 degassing and trigger wolframite precipitation due to a pH increase (Liu et al., 2018, Wood and Samson, 2000; Liu and Xiao, 2020; Wang et al., 2019, 2020b). Third, although pressure has a secondary effect on the transport and deposition of W-ore minerals, unmixing of CO_2 may indirectly promote the instability of W species by decreasing water activity and modifying the dielectric constant of the solvent, which controls ion paring (Kokh et al., 2017). Unmixing is recognized at Panasqueira (Portugal) W-ore deposit but only during the last

stages (noted IV following Cathelineau et al., 2020). Unmixing could have a role on W speciation and subsequently on the W precipitation, but it does not explain most of the wolframite precipitation at the very beginning of its formation under high pressure conditions, which excludes any unmixing process during early stages at Panasqueira.

5. Conclusions

The present study was based on in-situ Raman observations of W speciation in aqueous solutions loaded in fused silica capillary capsules (FSCC) at temperatures ranging from 25 to 400 °C and at different pH conditions. We identified four main W-species: (i) the tungstate anion $(WO_4)^{2-}$ which was found to be predominant at pH above 7.5 at 25 °C; (ii) the paratungstate A polyanion ($W_7O_{24}^{6-}$), which was found stable under circum-neutral conditions ($6 < pH < 7$) at $T \leq 100$ °C; (iii) the decatungstate Y-polyanion ($W_{10}O_{32}^{4-}$), a metastable polyanion, which predominates at a $pH < 5$ and $T \leq 200$ °C upon heating; and (iv) α-metatungstate (α-$[H_2W_{12}O_{40}]^{6-}$) which was the most abundant species at a $pH < 6$ and $T \geq 300$ °C.

Significant findings from this study are summarized below.

1) In aqueous solutions of highly soluble salts Na_2WO_4 and $Na_6W_{12}O_{39}$, tungsten polymers form reversibly under acidic to circum-neutral conditions and T up to 400 °C with a total tungsten concentration down to 0.01 m (~1700 ppm).

2) Tungsten does not form complexes with chloride and carbonate ions over the pH and T range investigated here ($0 < pH < 13$, 25 °C < T < 400 °C, 0.01m < W < 0.2m).

3) The W polymers identified under hydrothermal conditions are similar to those already well characterized at room T.

4) This work shifts the long-standing paradigm that highly-charged polymers cannot exist under hydrothermal conditions because of the decrease of the dielectric constant of water with T increase.

5) Thermodynamic constants for the three detected polytungstate anions are provided up to 300 °C. Our new data enabled the first quantitative predictions of the abundance of W polymers in geological fluids and allowed us to evaluate their role in W transport and deposition in ore deposits.

To constrain both electronic reorganization and nuclear quantum effects associated with oxygen bonding and polymerization, accurate ab initio molecular dynamics (AIMD) models are needed. Predicting the Raman spectra of the detected W polymers using density functional theory (DFT) will be essential for a full attribution of the W polymer Raman bands observed in this study.

Acknowledgements

We warmly acknowledge Associate editor Pr Jean François Boily for his work and the three anonymous reviewers for their very constructive reviews. We are grateful to Maria A. Kokh for her insightful discussion and precious advice along the course of this study. The authors also acknowledge Mr. Christopher Daly for the English verification. Pascal Robert and Aurélien Randi are warmly thanked for their help with the experimental setup. Guillaume Barre and Julien Boulliung are thanked for sharing their experiences and valuable suggestions on capillary loading techniques. Laurent Truche acknowledges support from the Institut Universitaire de France. This work was funded by the ERAMIN project NewOres funded by ANR (ANR-14-EMIN-0001), and Labex Ressources 21 (supported by the French National Research Agency through the national program "Investissements d'avenir") with reference ANR – 10 – LABX 21 —LABEX RESSOURCES 21.

References

Arnek, R., & Sasaki, Y. (1974). Equilibrium Studies of Polyanions. 20. A Recalculation of Emf Data on the Reactions of H^+ and WO_4^{2-} in 3 M $Na(ClO_4)$ at 25 °C. *Acta Chem. Scand. A*, 28(1).

Aveston, J. (1964). Hydrolysis of tungsten (VI): ultracentrifugation, acidity measurements, and Raman spectra of polytungstates.*Inorganic Chemistry*, *3*(7), 981-986.

Baes, C. F., & Mesmer, R. E. (1976). The Hydrolysis of Cations Wiley.*New York*, 177-182.

Bakker, R. J. (2018). AqSo_NaCl: Computer program to calculate pTVx properties in the H2O-NaCl fluid system applied to fluid inclusion research and pore fluid calculation. *Computers & geosciences*, *115*, 122-133.

Ball, T. K., Fortey, N. J., & Shepherd, T. J. (1985). Mineralisation at the Carrock Fell tungsten mine, N. England: paragenetic, fluid inclusion and geochemical study. *Mineralium Deposita*, *20*(1), 57-65

Barabanov, V. F. (1971). Geochemistry of tungsten. *International Geology Review*, *13*(3), 332-344

Barré, T., Arurault, L., & Sauvage, F. X. (2005). Chemical behavior of tungstate solutions: Part 1. A spectroscopic survey of the species involved. *Spectrochimica Acta Part A: Molecular and Biomolecular Spectroscopy*, *61*(4), 551-557.

Beuchat, S., Moritz, R. and Pettke, T., 2004. Fluid evolution in the W–Cu–Zn–Pb San Cristobal vein, Peru: fluid inclusion and stable isotope evidence. Chemical Geology, 210(1-4), pp.201-224.

Bilal, B. A., Haufe, P., & Möller, P. (1986). Raman spectroscopic and electrochemical study of polymerization of tungsten (VI) in a hydrothermal solution up to 1 kbar and 200 C. *Physica B+ C*, *139*, 721-724.

Brimhall, G.H. & Crerar, D.A., (1987). Ore fluids: magmatic to supergene. In: I.S.E. Carmichael and H.P. Eugster (Editors), Thermodynamic Modelling of Geochemical Materials: Minerals, Fluids and Melts. *Rev. Mineral., 17:* 235-321.

Brugger, J., Liu, W., Etschmann, B., Mei, Y., Sherman, D. M., & Testemale, D. (2016). A review of the coordination chemistry of hydrothermal systems, or do coordination changes make ore deposits? *Chemical Geology, 447*, 219-253.

Cathelineau, M., Boiron, M., Marignac, C., Dour, M., Dejean, M., Carocci, E., Truche, L., & Pinto, F. (2020). High pressure and temperatures during the early stages of tungsten deposition at Panasqueira revealed by fluid inclusions in topaz. *Ore Geology Reviews, 126*, 103741.

Caumon, M. C., Dubessy, J., Robert, P., & Tarantola, A. (2013). Fused-silica capillary capsules (FSCCs) as reference synthetic aqueous fluid inclusions to determine chlorinity by Raman spectroscopy. *European Journal of Mineralogy*, *25*(5), 755-763.

Chou I.-M., Song Y. & Burruss R. C. (2008). A new method for synthesizing fluid inclusions in fused silica capillaries containing organic and inorganic material. *Geochim. Cosmochim. Acta* 72, 5217–5231.

Crerar, D., Wood, S., Brantley, S., & Bocarsly, A. (1985). Chemical controls on solubility of ore-forming minerals in hydrothermal solutions. *Canadian Mineralogist*, *23*(3), 333-352.

Cruywagen, J. J., & Van Der Merwe, I. F. (1987). Tungsten (VI) equilibria: a potentiometric and calorimetric investigation. *Journal of the Chemical Society, Dalton Transactions*, (7), 1701-1705.

Cruywagen, J. J. (1999). Protonation, oligomerization, and condensation reactions of vanadate (V), molybdate (VI), and tungstate (VI). In *Advances in inorganic chemistry* (Vol. 49, pp. 127-182). Academic Press.

Dargent, M., Dubessy, J., Truche, L., Bazarkina, E. F., Nguyen-Trung, C., & Robert, P. (2013). Experimental study of uranyl (VI) chloride complex formation in acidic LiCl aqueous solutions under hydrothermal conditions (T= 21 C–350 C, Psat) using Raman spectroscopy. *European Journal of Mineralogy*, *25*(5), 765-775.

Driesner, T. (2007). The system H2O–NaCl. Part II: Correlations for molar volume, enthalpy, and isobaric heat capacity from 0 to 1000 C, 1 to 5000 bar, and 0 to 1 XNaCl. *Geochimica et Cosmochimica Acta*, *71*(20), 4902-4919.

Driesner, T., & Heinrich, C. A. (2007). The system H2O–NaCl. Part I: Correlation formulae for phase relations in temperature–pressure–composition space from 0 to 1000 C, 0 to 5000 bar, and 0 to 1 XNaCl. *Geochimica et Cosmochimica Acta*, *71*(20), 4880-4901.

Duncan, J. F., & Kepert, D. L. (1961). 1050. Polyanion equilibria in aqueous solution. Part I. The quantitative analysis of acidified tungstate solutions. *Journal of the Chemical Society (Resumed)*, 5317-5325.

Eugster H. P. & Wilson G. A. (1985). Transport and deposition of ore-forming elements in hydrothermal systems associated with granites. In High Heat Production Granites, Hydrothermal Circulation and Ore Genesis. *Inst. Min. Metall., London*, pp. 87-98.

Fuchs, J., & Flindt, E. P. (1979). Preparation and structure investigation of polytungstates-contribution to the paratungstate-a problem. *Zeitschrift fur Naturforschung Section Ba Journal of Chemical Sciences*, *34*(3), 412-422.

Fusswinkel, T., Wagner, T., & Sakellaris, G. (2017). Fluid evolution of the Neoarchean Pampalo orogenic gold deposit (E Finland): Constraints from LA-ICPMS fluid inclusion microanalysis. *Chemical Geology*, *450*, 96-121.

Gibert, F., Moine, B., Schott, J., & Dandurand, J. L. (1992). Modeling of the transport and deposition of tungsten in the scheelite-bearing calc-silicate gneisses of the Montagne Noire, France. *Contributions to Mineralogy and Petrology*, *112*(2-3), 371-384.

Goldmann, S., Melcher, F., Gäbler, H. E., Dewaele, S., Clercq, F. D., & Muchez, P. (2013). Mineralogy and trace element chemistry of ferberite/reinite from tungsten deposits in central Rwanda. *Minerals*, *3*(2), 121-144.

Gumerova, N.I., & Rompel, A. (2020). Polyoxometalates in solution: speciation under spotlight. *Chemical Society Reviews, 49*(21), pp.7568-7601.

Guo, Q., Li, Y., & Luo, L. (2019). Tungsten from typical magmatic hydrothermal systems in China and its environmental transport. *Science of The Total Environment*, *657*, 1523-1534.

Hartl, H., Palm, R., & Fuchs, J. (1993). Ein neuer Parawolframat-Typ. *Angewandte Chemie*, *105*(10), 1545-1547.

Hastings, J. J., & Howarth, O. W. (1992). A 183W, 1H and 17O nuclear magnetic resonance study of aqueous isopolytungstates. *Journal of the Chemical Society, Dalton Transactions*, (2), 209-215.

Häufe, P. (1982). Raman-spectrophotometric determination of the tungstate anion and its isopolyanions in aqueous systems. *Fresenius' Zeitschrift für analytische Chemie*, *310*(5), 388-391.

Heinrich, C. A. (1990). The chemistry of hydrothermal tin (-tungsten) ore deposition. *Economic Geology*, *85*(3), 457-481.

Higgins, N. C. (1980). Fluid inclusion evidence for the transport of tungsten by carbonate complexes in hydrothermal solutions. *Canadian Journal of Earth Sciences, 17*(7), 823-830.

Himeno, S., Yoshihara, M., & Maekawa, M. (2000). Formation of voltammetrically-active isopolyoxotungstate complexes in aqueous CH3CN media. *Inorganica Chimica Acta*, *298*(2), 165-171.

Himeno, S., & Kitazumi, I. (2003). Capillary electrophoretic study on the formation and transformation of isopolyoxotungstates in aqueous and aqueous-CH3CN media. *Inorganica chimica acta*, *355*, 81-86.

Hulsbosch, N., Boiron, M. C., Dewaele, S., & Muchez, P. (2016). Fluid fractionation of tungsten during granite–pegmatite differentiation and the metal source of peribatholitic W quartz veins: Evidence from the Karagwe-Ankole Belt (Rwanda). *Geochimica et Cosmochimica Acta*, *175*, 299-318.

Jander, G., Mojert, D., & Aden, T. (1929). Über amphotere Oxydhydrate, deren wäßrige Lösungen und kristallisierende Verbindungen. VIII. Mitteilung. Über Wolframate, Isopoly-und Heteropoly-Wolframsäuren. *Zeitschrift für anorganische und allgemeine Chemie, 180*(1), 129-149.

Kokh, M. A., Akinfiev, N. N., Pokrovski, G. S., Salvi, S., & Guillaume, D. (2017). The role of carbon dioxide in the transport and fractionation of metals by geological fluids. *Geochimica et Cosmochimica Acta*, *197*, 433-466.

Klemme, S., Feldhaus, M., Potapkin, V., Wilke, M., Borchert, M., Louvel, M., ... & Testemale, D. (2021). A hydrothermal apparatus for x-ray absorption spectroscopy of hydrothermal fluids at DESY. *Review of Scientific Instruments*, *92*(6), 063903.

Korges, M., Weis, P., Lüders, V. & Laurent, O. (2018). Depressurization and boiling of a single magmatic fluid as a mechanism for tin-tungsten deposit formation. *Geology*, *46*(1), pp.75-78.

Liu, Z., Mao, X., Deng, H., Li, B., Zhang, S., Lai, J., ... & Shang, Q. (2018). Hydrothermal processes at the Axi epithermal Au deposit, western Tianshan: insights from geochemical effects of alteration, mineralization and trace elements in pyrite. *Ore Geology Reviews*, *102*, 368-385.

Liu, X., & Xiao, C. (2020). Wolframite solubility and precipitation in hydrothermal fluids: insight from thermodynamic modeling. *Ore Geology Reviews*, *117*, 103289.

Maksimovskaya, R. I., & Burtseva, K. G. (1985). 17O and 183W NMR studies of the paratungstate anions in aqueous solutions. Polyhedron, 4(9), 1559-1562.

Mei, J., & Bao, Z. (2014). Side chain engineering in solution-processable conjugated polymers. *Chemistry of Materials*, *26*(1), 604-615.

Naumov, V. B., Dorofeev, V. A., & Mironova, O. F. (2011). Physicochemical parameters of the formation of hydrothermal deposits: a fluid inclusion study. I. Tin and tungsten deposits. *Geochemistry International*, *49*(10), 1002-1021.

Ng, K. Y. S., & Gulari, E. (1984). Spectroscopic and scattering investigation of isopoly-molybdate and tungstate solutions. *Polyhedron*, *3*(8), 1001-1011.

Ni, P., Wang, X. D., Wang, G. G., Huang, J. B., Pan, J. Y., & Wang, T. G. (2015). An infrared microthermometric study of fluid inclusions in coexisting quartz and wolframite from Late Mesozoic tungsten deposits in the Gannan metallogenic belt, South China. *Ore Geology Reviews*, *65*, 1062-1077.

Pope, M. T. (1983). Heteropoly and isopoly oxometalates. *Springer-Verlag*.

Redkin, A. F., & Bondarenko, G. V. (2010). Raman spectra of tungsten-bearing solutions. *Journal of solution chemistry*, *39*(10), 1549-1561.

Redkin A. F., & Cygan G. L. (2020). Experimental Determination of Ferberite Solubility in the KCl–HCl–H_2O System at 400–500 °C and 20–100 MPa. In: Litvin Y., Safonov O. (eds) Advances in Experimental and Genetic Mineralogy. *Springer Mineralogy*. Springer, Cham. https://doi.org/10.1007/978-3-030-42859-4_7

Rios, F. J., Villas, R. N., & Fuzikawa, K. (2003). Fluid evolution in the Pedra Preta wolframite ore deposit, Paleoproterozoic Musa granite, eastern Amazon craton, Brazil. *Journal of South American Earth Sciences*, *15*(7), 787-802.

Ross-Medgaarden, E. I., & Wachs, I. E. (2007). Structural determination of bulk and surface tungsten oxides with UV− vis diffuse reflectance spectroscopy and raman spectroscopy. *The Journal of Physical Chemistry C*, *111*(41), 15089-15099.

Shvarov, Y. V. (2008). HCh: New potentialities for the thermodynamic simulation of geochemical systems offered by Windows. *Geochemistry International*, 46, 834-839.

Truche, L., Bazarkina, E. F., Barré, G., Thomassot, E., Berger, G., Dubessy, J., & Robert, P. (2014). The role of S− 3 ion in thermochemical sulphate reduction: Geological and geochemical implications. *Earth and Planetary Science Letters*, *396*, 190-200.

Vigasina, M. F., Orlov, R. Y., Dadze, T. P., & Kashirtseva, G. A. (2000). Determination of thermodynamic parameters of water-dissolved complexes at T< 360oC with the help of Raman spectroscopy: methods and equipment. In *Raman Scattering* (Vol. 4069, pp. 103-108). International Society for Optics and Photonics.

Wang, X. S., Timofeev, A., Williams-Jones, A. E., Shang, L. B., & Bi, X. W. (2019). An experimental study of the solubility and speciation of tungsten in NaCl-bearing aqueous solutions at 250, 300, and 350° C. *Geochimica et Cosmochimica Acta*.

Wang, X., Qiu, Y., Lu, J., Chou, I. M., Zhang, W., Li, G., & Zhong, R. (2020a). In situ Raman spectroscopic investigation of the hydrothermal speciation of tungsten: Implications for the ore-forming process. *Chemical Geology*, 119299.

Wang, X., Qiu Y., Chou, I. M., Zhang, R., Li G., & Zhong, R. (2020b). Effects of pH and Salinity on the Hydrothermal Transport of Tungsten: Insights from In Situ Raman Spectroscopic Characterization of K_2WO_4 – NaCl – HCl - CO_2 Solutions at Temperatures up to 400°C. *Geofluids*. ID 2978984, 12 pages, 2020. https://doi.org/10.1155/2020/2978984

Weiner, H., Lunk, H. J., Friese, R., & Hartl, H. (2005). Synthesis, Crystal Structure, and Solution Stability of Keggin-Type Heteropolytungstates (NH4) 6NiII0. 5 [α-FeIIIO4W11O30NiIIO5 (OH2)]⊙ n H2O,(NH4) 7Zn0. 5 [α-ZnO4W11O30ZnO5 (OH2)]⊙ n H2O, and (NH4) 7NiII0. 5 [α-ZnO4W11O30NiIIO5 (OH2)]⊙ n H2O (n≈ 18). *Inorganic chemistry*, *44*(22), 7751-7761.

Wesolowski, D., Drummond, S. E., Mesmer, R. E., & Ohmoto, H. (1984). Hydrolysis equilibria of tungsten (VI) in aqueous sodium chloride solutions to 300. degree. C. *Inorganic Chemistry*, *23*(8), 1120-1132.

Wood, S. A., & Vlassopoulos, D. (1989). Experimental determination of the hydrothermal solubility and speciation of tungsten at 500° C and 1 kbar1, 2. *Geochimica et Cosmochimica Acta*, 53(2), 303-312.

Wood, S. A. (1992). Experimental determination of the solubility of WO3 (s) and the thermodynamic properties of H2WO4 (aq) in the range 300–600 C at 1 kbar: calculation of scheelite solubility. *Geochimica et Cosmochimica Acta*, 56(5), 1827-1836.

Wood, S. A., & Samson, I. M. (2000). The hydrothermal geochemistry of tungsten in granitoid environments: I. Relative solubilities of ferberite and scheelite as a function of T, P, pH, and m NaCl. *Economic Geology*, *95*(1), 143-182.

Zhang, Y., Yang, J. H., Chen, J. Y., Wang, H., & Xiang, Y. X. (2017). Petrogenesis of Jurassic tungsten-bearing granites in the Nanling Range, South China: Evidence from whole-rock geochemistry and zircon U–Pb and Hf–O isotopes. Lithos, 278, 166-180.

Figure Captions

Fig.1: Raman spectra of dissolved W-species in hydrothermal solution #5 (0.1 m W from $Na_6W_{12}O_{39}$, H_2O + 0.1 m NaCl, $pH_{25°C}$=5.60) as a function of temperature.

Fig.2: (A) Raman spectra between 850 cm^{-1} and 980 cm^{-1} of solution #10 (0.1m W from $Na_2WO_4{\cdot}2H_2O$ + 0.1 m NaOH) from 25 °C, up to 400 °C showing the band of tungstate ion B $(WO_4)^{2-}$. **(B)** Raman spectra showing the band of tungstate ion $(WO_4)^{2-}$ (species B) at 200°c and for different total tungsten concentrations: 0.01 m, 0.05 m, 0.1 m, 0.2 m. The intensity of $(WO_4)^{2-}$ Raman band increases with W-concentration. **(C)** Linear correlation between the "B" species (WO_4^{2-}) Raman band area normalized to the water bending band area and tungsten volumetric concentration for different temperatures from 25 to 400 °C. The line slope stands for the calibration coefficient K_T (in $mol{\cdot}L^{-1}$) at a given temperature for $(WO_4)^{2-}$ ion. **(D)** Relationship between the calibration coefficient K_T of $(WO_4)^{2-}$ ion and temperature.

Fig. 3: Raman spectra of four different W-bearing aqueous solution at four different pH conditions and at temperature ranging from 25 to 400 °C. **(A)** Hyper-alkaline condition (solution #10, 0.1m total W concentration from $Na_2WO_4{\cdot}2H_2O$ + 0.1m NaOH, pH = 13.02 at 25 °C) characterized by the dissolution of only one isolated species. **(B)** Circumneutral condition (solution #2, 0.1 m total W concentration from $Na_2WO_4{\cdot}2H_2O$ + 0.1 m HCl. pH = 6.87 at 25 °C. **(C)** Slightly acidic condition (solution #5, 0.1 m total W concentration from $Na_6W_{12}O_{39}{\cdot}H_2O$ + 0.1 m NaCl, pH = 5.60 at 25 °C). **(D)** Strongly acidic condition (solution #1, 0.1 m total W concentration from $Na_6W_{12}O_{39}{\cdot}H_2O$ + 0.1 m HCl, pH = 1.10 at 25 °C). (E) Microscopic image of FSCC containing 0.1 m total W concentration from $Na_6W_{12}O_{39}{\cdot}H_2O$ + 0.1 m NaCl at T= 300 °C, showing the precipitation of W-bearing solid phases.

Fig. 4: Raman spectra for the solution #R1 (0.1 m total W concentration from $Na_2WO_4{\cdot}2H_2O$ + 0.5 m CH_3COOH; $pH_{T=25°C}$= 4.00). **(A)** W-speciation for fresh solution at T = 25 °C (blue), immediately after heating at 200 °C (purple), 300 °C (orange) and 400 °C (red), and at T = 25 °C immediately after cooling (light blue) and two months after cooling (fuchsia). The blue spectrum in the upper part represents the W-speciation of the unheated solution after six months at 25 °C. **(B)** Shows Raman spectra collected at various T on the same solution but after a pre-heating at 350 °C for two days.

Fig. 5: Raman spectra showing the effect of W concentration (0.01 and 0.1 m total W concentration) on W speciation at temperature ranging from 25 to 400 °C and pH buffered by 0.5 m acetic acid (pH ~ 4 at 25 °C). **(A)** Solution #18: 0.01 m total W concentration from $Na_2WO_4{\cdot}2H_2O$ + 0.5 m CH_3COOH, $pH_{25°C}$ = 3.57. **(B)** Solution #R1: 0.10 m total W concentration from $Na_2WO_4{\cdot}2H_2O$ + 0.5 m CH_3COOH $pH_{25°C}$ = 4.00. Tungsten speciation is unchanged whatever the temperature within this W concentration range.

Fig. 6: Raman spectra of W-bearing aqueous solutions in carbonate-bearing systems at 3 contrasted pH conditions and at temperatures ranging from 25 to 400°C. **(A)** Circum-neutral condition (solution #12, 0.1 m total W concentration from $Na_2WO_4{\cdot}2H_2O$ + 0.14 m CO_2, calculated pH = 7.2 at 25 °C). **(B)** Alkaline condition (solution #11, 0.1 m total W concentration from $Na_2WO_4{\cdot}2H_2O$ + 1.1m $NaHCO_3$, pH = 8.30 at 25°C). (C) Hyper alkaline condition (solution #13, 0.1 m total W concentration from $Na_2WO_4{\cdot}2H_2O$ + 1.2 m Na_2CO_3, pH = 11.85 at 25°C).

Fig. 7: Raman spectra of W-bearing aqueous solutions in chloride-bearing systems (NaCl) systems, from 25 to 400 °C. In **(A)** acidic condition (solution #14, 0.1 m total W concentration from $Na_2WO_4{\cdot}2H_2O$ + 3.5 m NaCl + 0.5 m CH_3COOH, pH = 5.28 at 25 °C). **(B)** Alkaline condition (solution #8, 0.1 m total W concentration from $Na_2WO_4{\cdot}2H_2O$ + 3.6 NaCl, pH= 9.56 at 25°C).

Fig. 8: Tungsten speciation as a function of pH and temperature as deduced from a quantitative interpretation of the Raman spectra. **(A)** 25 °C, **(B)** 100°C, **(C)** 200°C, **(D)** 300 °C. The total W concentration is 0.1 m.

Fig. 9: Distribution in different W aqueous species at 300°C and P_{sat} as a function of pH at 0.1m total W concentration and 0.1m NaCl: **(A)** as determined from Raman spectroscopy data obtained in this study, and **(B)** considering the HWO_4^{2-} and $H_2WO_4^0{}_{(aq)}$ from the literature. **(C)** The relative importance of W species in aqueous fluids with 1m NaCl and variable concentration of dissolved Na_2WO_4 as a function of pH and total W concentration under 300°C and saturated vapour pressure. The lines correspond to the equality of mW in polymers and mW in other forms; the blue area indicates the conditions of W polymer predominance; the blue vertical dashed line indicates the neutral pH value at 300°C (5.70), the blue horizontal flesh indicates W concentration 1 ppm ($5.8{\cdot}10^{-6}$ mW). **(D)** The solubility of scheelite ($CaWO_4$) as a function of pH at 300°C in 5m NaCl aqueous solution and the concentrations of different species types. The stability of HWO_4^{2-} and $H_2WO_4^0{}_{(aq)}$ in **(B)**, **(C)**, and **(D)** is taken according to Wang et al. (2019). The grey field indicated the pH when WO_3 can precipitate; the residual W concentration is below $5{\cdot}10^{-4}$ m.

Declaration of interests

☒ The authors declare that they have no known competing financial interests or personal relationships that could have appeared to influence the work reported in this paper.

☐The authors declare the following financial interests/personal relationships which may be considered as potential competing interests:

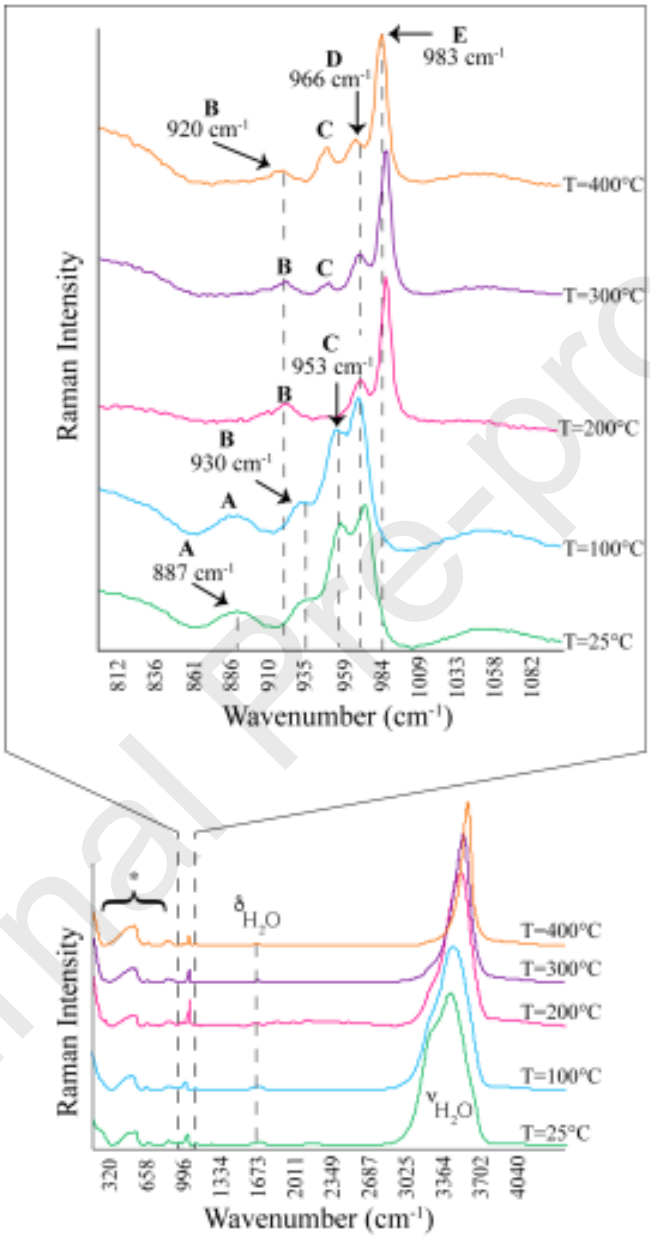

* Band of silica glass of the FSCC

Fig. 1

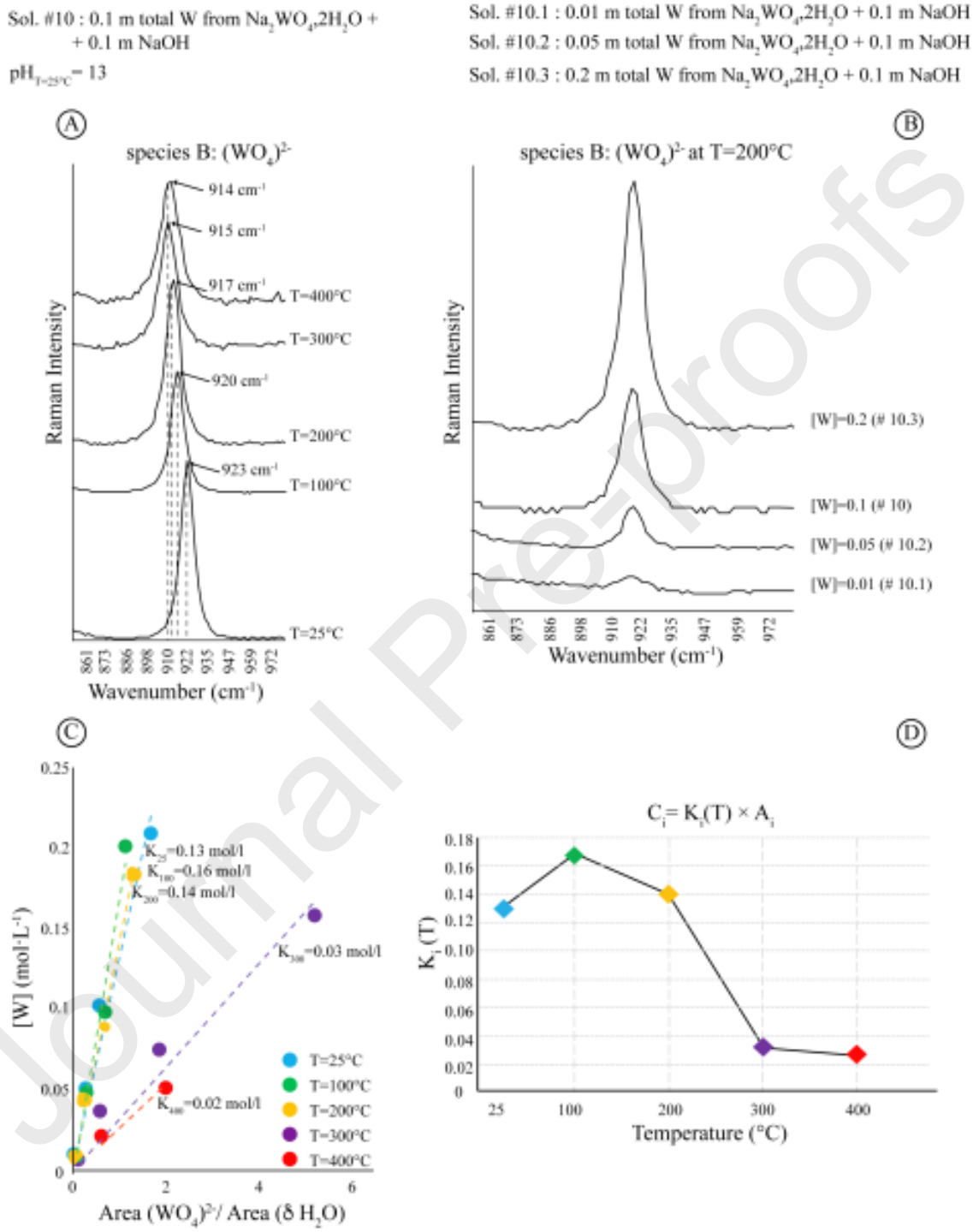

Fig. 2

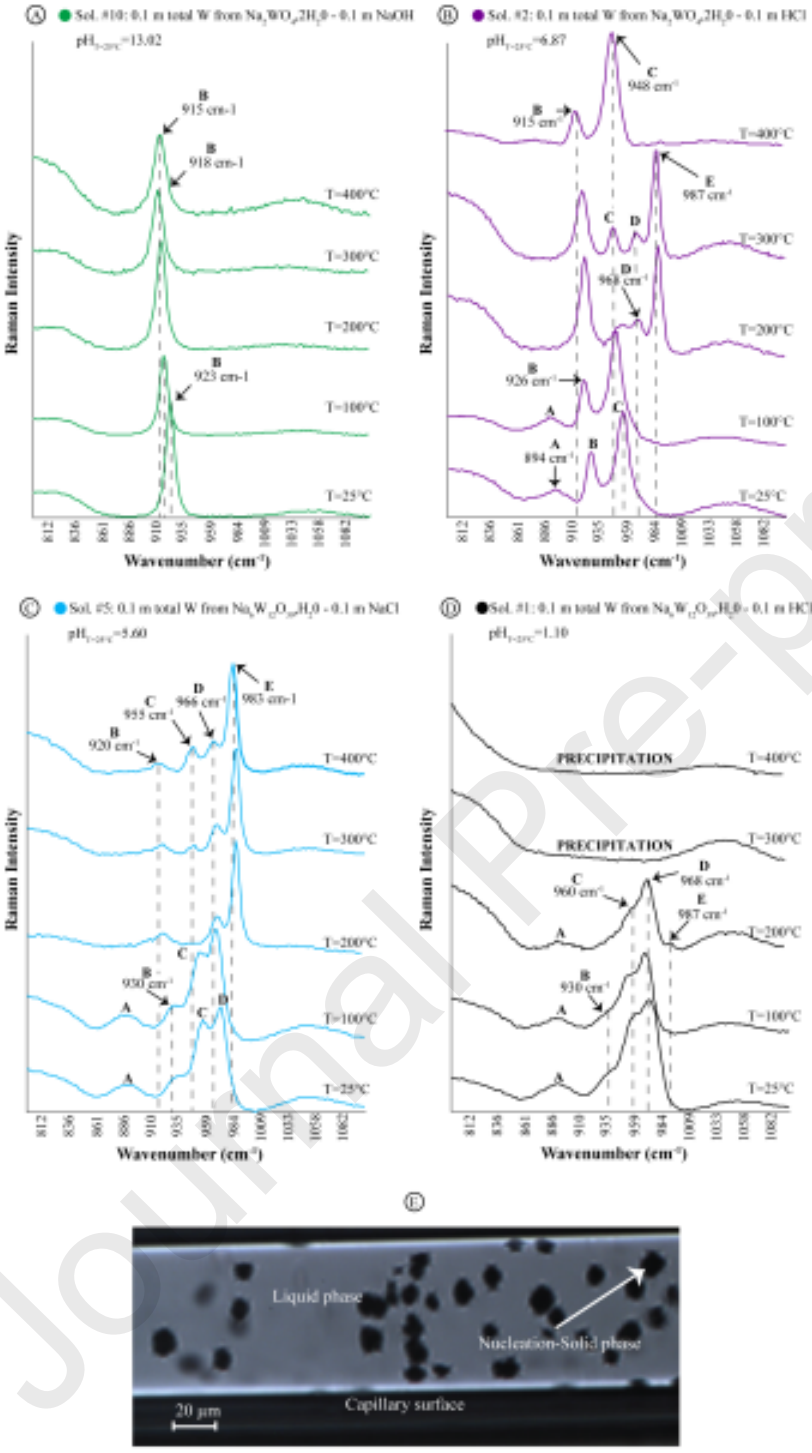
Ⓐ Sol. #10: 0.1 m total W from Na2WO4·2H2O - 0.1 m NaOH
pH T-25°C=13.02
B 915 cm-1
B 918 cm-1
B 923 cm-1
T=400°C
T=300°C
T=200°C
T=100°C
T=25°C
Raman Intensity
Wavenumber (cm-1)
Ⓑ Sol. #2: 0.1 m total W from Na2WO4·2H2O - 0.1 m HCl
pH T-25°C=6.87
B 915 cm-1
C 948 cm-1
E 987 cm-1
C
D
D 968 cm-1
B 926 cm-1
A
C
A 894 cm-1
B
T=400°C
T=300°C
T=200°C
T=100°C
T=25°C
Raman Intensity
Wavenumber (cm-1)
Ⓒ Sol. #5: 0.1 m total W from Na2W12O39·H2O - 0.1 m NaCl
pH T-25°C=5.60
B 920 cm-1
C 955 cm-1
D 966 cm-1
E 983 cm-1
B 930 cm-1
A
C
D
A
T=400°C
T=300°C
T=200°C
T=100°C
T=25°C
Raman Intensity
Wavenumber (cm-1)
Ⓓ Sol. #1: 0.1 m total W from Na2W12O39·H2O - 0.1 m HCl
pH T-25°C=1.10
PRECIPITATION
PRECIPITATION
C 960 cm-1
D 968 cm-1
E 987 cm-1
A
B 930 cm-1
A
A
T=400°C
T=300°C
T=200°C
T=100°C
T=25°C
Raman Intensity
Wavenumber (cm-1)
Ⓔ
Liquid phase
Nucleation-Solid phase
Capillary surface
20 µm

Fig. 3

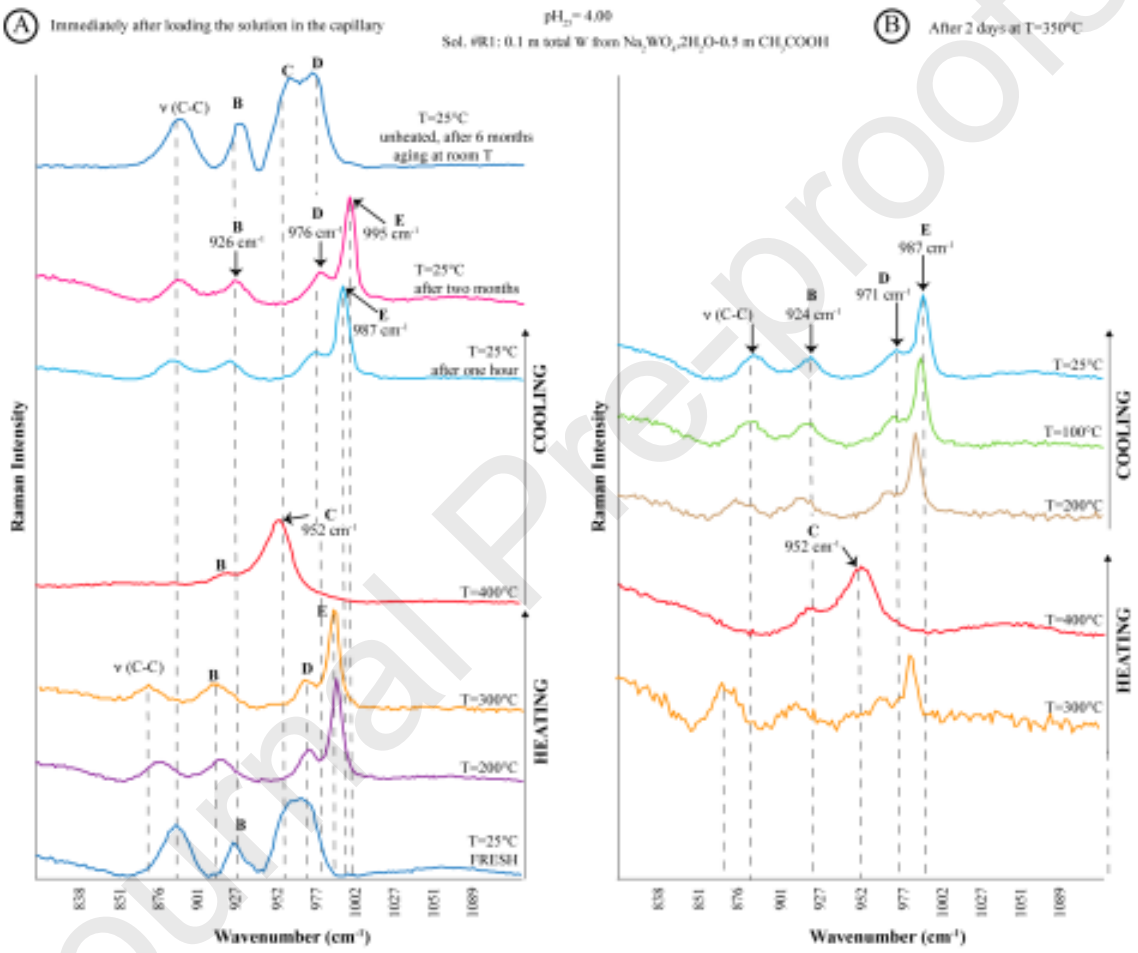
A
Immediately after loading the solution in the capillary
pH_RT = 4.00
Sol. #R1: 0.1 m total W from Na2WO4·2H2O-0.5 m CH3COOH
B
After 2 days at T=350°C
ν (C-C)
B
C
D
E
T=25°C
unheated, after 6 months
aging at room T
926 cm⁻¹
976 cm⁻¹
995 cm⁻¹
T=25°C
after two months
987 cm⁻¹
T=25°C
after one hour
952 cm⁻¹
T=400°C
T=300°C
T=200°C
T=25°C
FRESH
COOLING
HEATING
Raman Intensity
838
851
876
901
927
952
977
1002
1027
1051
1089
Wavenumber (cm⁻¹)
924 cm⁻¹
971 cm⁻¹
987 cm⁻¹
952 cm⁻¹
T=100°C

Fig. 4

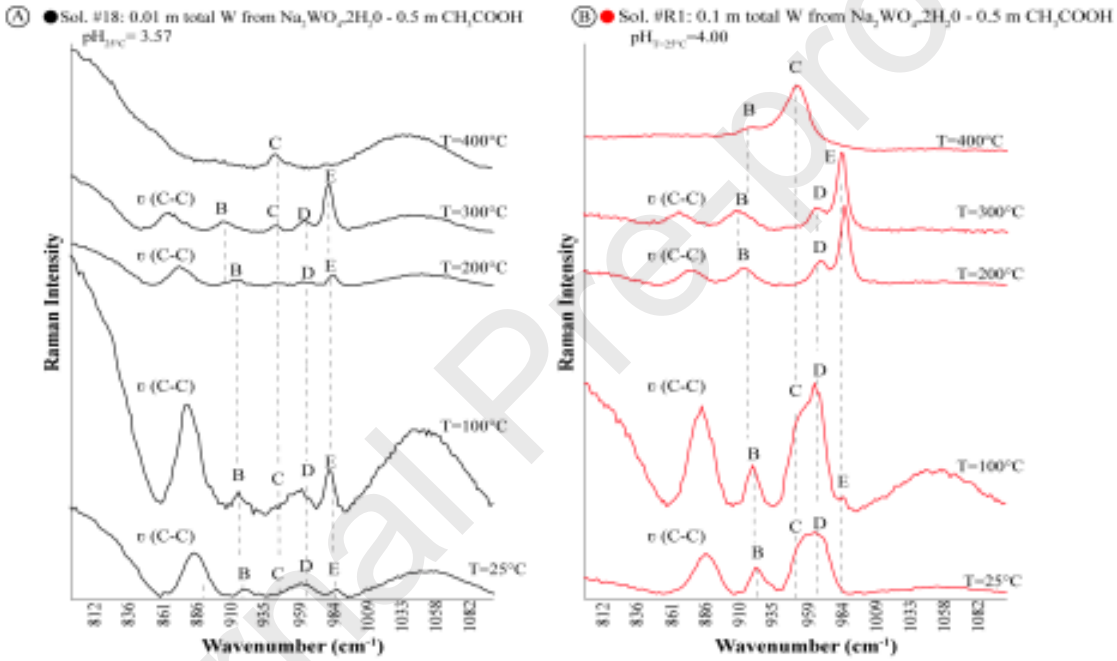
A
Sol. #18: 0.01 m total W from Na2WO4·2H2O - 0.5 m CH3COOH
pH25°C= 3.57
B
Sol. #R1: 0.1 m total W from Na2WO4·2H2O - 0.5 m CH3COOH
pH25°C=4.00
Raman Intensity
Wavenumber (cm-1)
T=400°C
T=300°C
T=200°C
T=100°C
T=25°C
υ (C-C)
812
836
861
886
910
935
959
984
1009
1033
1058
1082

Fig. 5

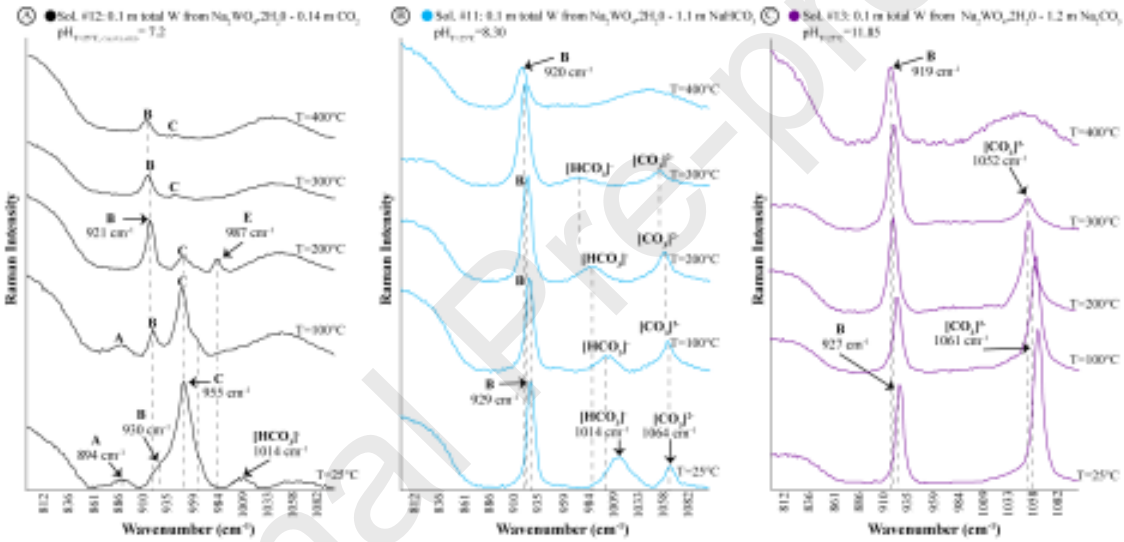
Raman Intensity
Wavenumber (cm⁻¹)
T=400°C
T=300°C
T=200°C
T=100°C
T=25°C
B
C
E
A
921 cm⁻¹
987 cm⁻¹
955 cm⁻¹
930 cm⁻¹
894 cm⁻¹
[HCO3]⁻
1014 cm⁻¹
920 cm⁻¹
929 cm⁻¹
[CO3]²⁻
1064 cm⁻¹
919 cm⁻¹
1052 cm⁻¹
927 cm⁻¹
1061 cm⁻¹

Fig. 6

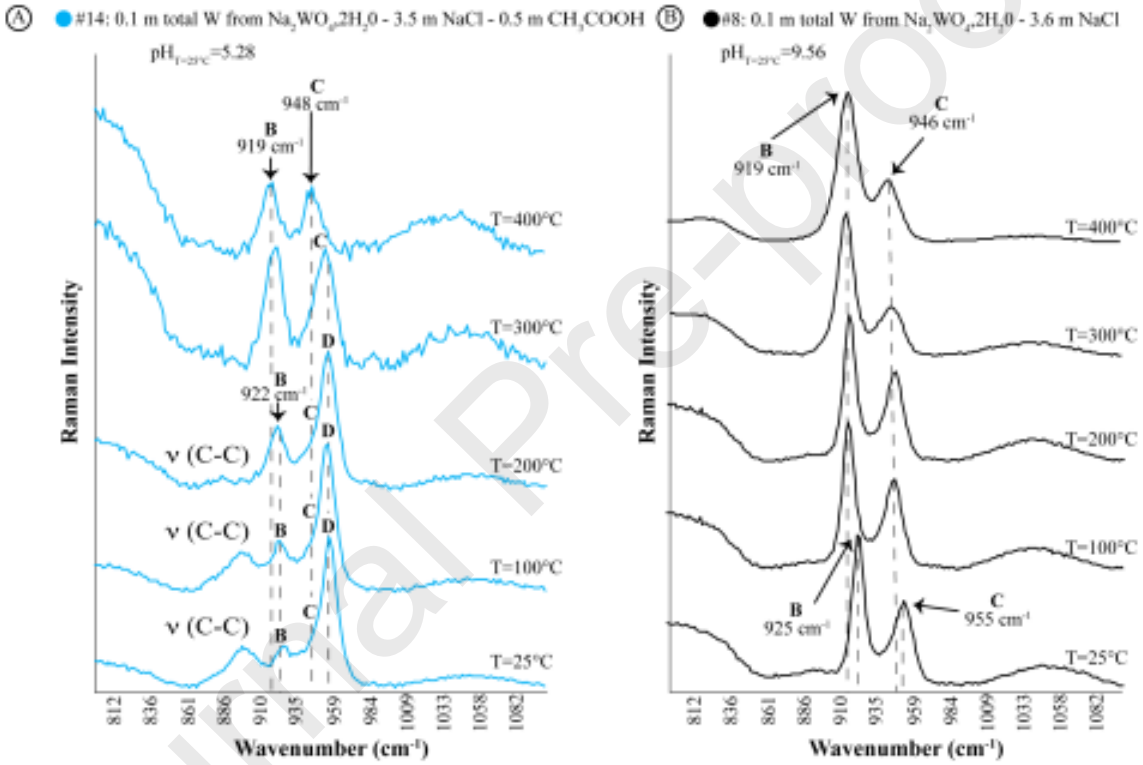

Fig. 7

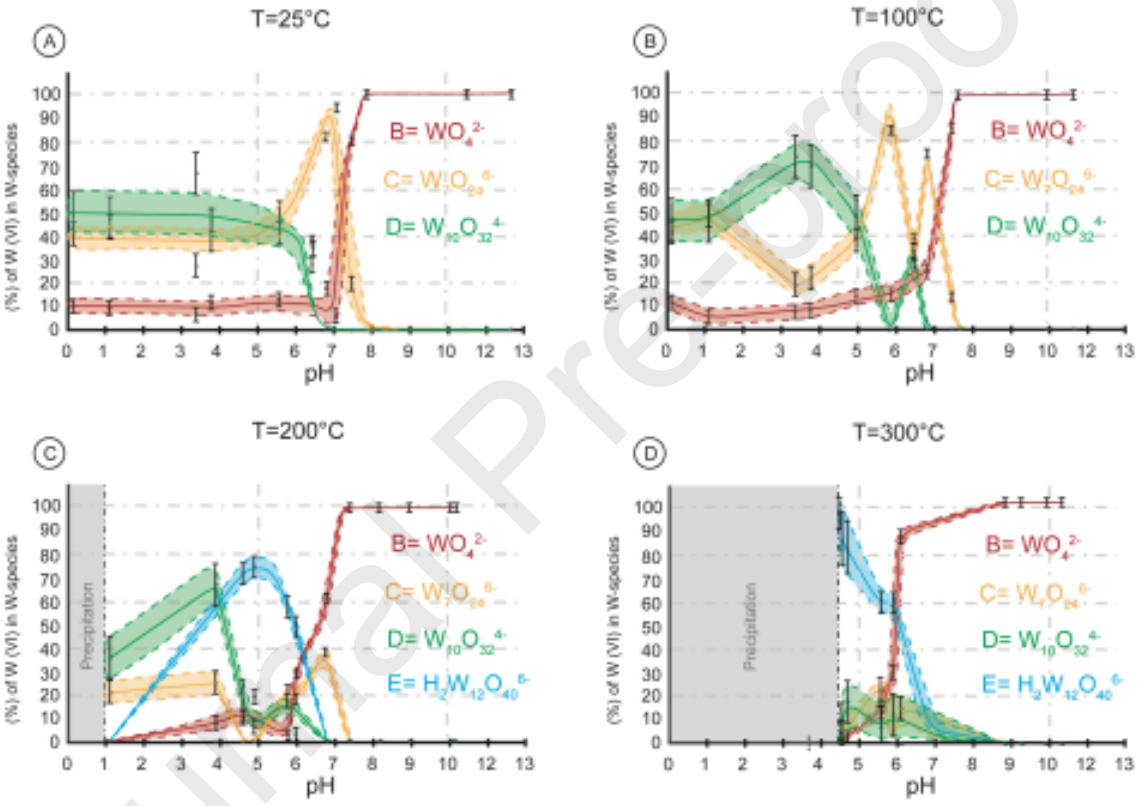
T=25°C
T=100°C
T=200°C
T=300°C
(%) of W (VI) in W-species
pH
Precipitation
B= WO4 2-
C= W7O24 6-
D= W10O32 4-
E= H2W12O40 6-

Fig. 8

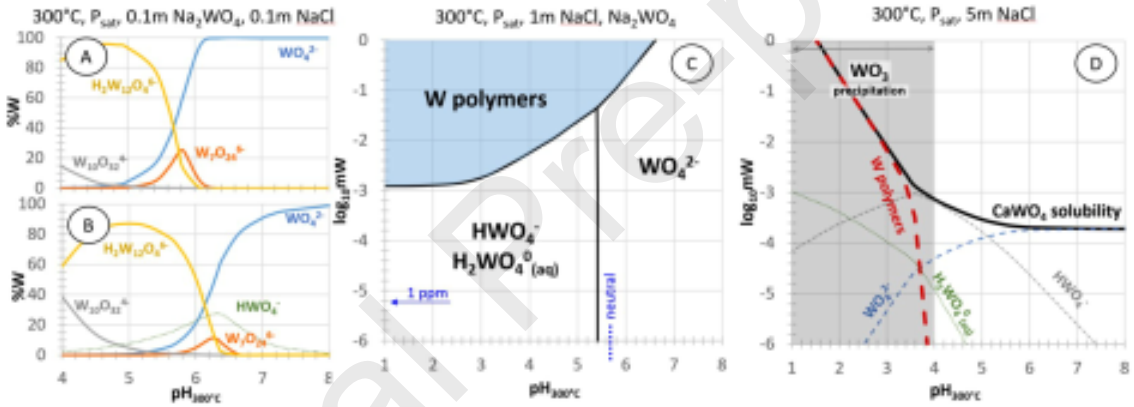
300°C, P_sat, 0.1m Na2WO4, 0.1m NaCl
A
B
%W
pH300°C
300°C, P_sat, 1m NaCl, Na2WO4
C
W polymers
WO4 2-
HWO4-
H2WO4 0 (aq)
1 ppm
neutral
log10mW
pH300°C
300°C, P_sat, 5m NaCl
D
WO3 precipitation
W polymers
CaWO4 solubility
WO4 2-
HWO4-
log10mW
pH300°C

Fig. 9

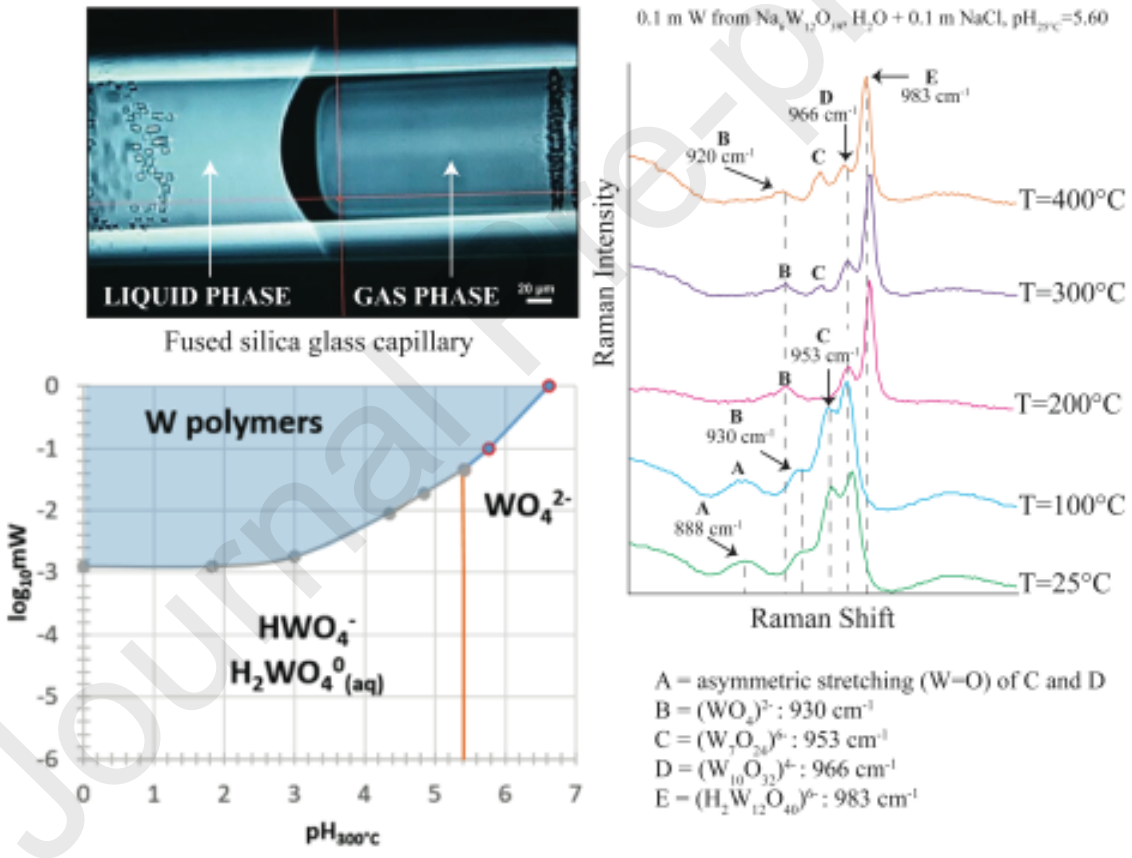

Graphical Abstract